Article:
Pugliese, F., De Risi, R. and Di Sarno, L. (2022) Reliability assessment of existing RC bridges with spatially-variable pitting corrosion subjected to increasing traffic demand. Reliability Engineering & System Safety, 218 (Part A). 108137. ISSN: 0951-8320

https://doi.org/10.1016/j.ress.2021.108137

Reliability assessment of existing RC bridges with spatially-variable pitting corrosion subjected to increasing traffic demand

Pugliese, F., [a] De Risi, R. [b] and Di Sarno, L. [c]

[a]*Institute for Risk and Uncertainty and Department of Civil Engineering and Industrial Design, School of Engineering, University of Liverpool, Liverpool, UK.* Email address: Francesco.Pugliese@liverpool.ac.uk.

[b]*Civil Engineering, Department of Civil Engineering, University of Bristol, Bristol, UK.* Email address: raffaele.derisi@bristol.ac.uk

[c]*Department of Civil Engineering and Industrial Design, School of Engineering, University of Liverpool, Liverpool, UK.* Email address: luigi.di-sarno@liverpool.ac.uk; *Department of Engineering, University of Sannio, Benevento, Italy*.

Corresponding author: Francesco.Pugliese@liverpool.ac.uk.

Abstract:
Bridges are critical for transportation networks. Temporary closures due to poor maintenance may trigger adverse cascading events, affecting economic and societal well-being. Two main factors play a key role in bridge health conditions: ageing and wear-and-tear due to the increasing traffic. This paper proposes a comprehensive framework to quantify the combined phenomena in a holistic approach. The reliability assessment of an existing reinforced concrete bridge subjected to increasing traffic demand and spatially-variable pitting corrosion is investigated. Empirical data are used to develop probabilistic models for cracking initiation, pitting factor, severe cracking, and cover spalling.
Statistical distributions of temperatures from a local meteorological station are used to investigate environmental effects on corrosion initiation. For the traffic, national highway databases are used to model the vehicular flow. Ductile and brittle failure mechanics are considered for the structural capacity assessment. Coupled biaxial bending-axial loading domain is adopted for the ductile structural checks. The shear capacity is assessed through the response limit surface from the modified compression field theory results. Finally, Monte Carlo simulations are performed at intervals of 10 years to derive a time-dependent reliability profile compared against standard thresholds to determine the health conditions of the bridge.

Keywords: Reliability Assessment; Corrosion; Probabilistic Modelling; Traffic loading; Bridge Engineering.

1. INTRODUCTION

Many reinforced concrete (RC) bridges worldwide were designed in the 60s and are now experiencing damage due to the exposure to aggressive environmental agents and increasing live loading (i.e., the severe increment of traffic volume) [e.g., Enright and Frangopol (1998), Ellingwood (2005); Choe et al. (2009); Yang and Frangopol (2020)]. The continuous growth of such service loadings and the decay of the concrete and steel bar mechanical properties may significantly impact the residual capacity of existing RC infrastructure [e.g., Kumar et al. (2009); Simon et al. (2010); Ghosh and Padgett (2010)].

Often, poor or lack of maintenance reduces the expected service life of bridges and, in extreme cases, may lead to structural collapse. Thus, advanced reliability procedures are required to assess the residual capacity of aged RC infrastructure.

The risk assessment of bridges under environmental and traffic loadings involves many epistemic and aleatoric uncertainties. [e.g., Celik and Ellingwood (2010); Pan et al. (2011); Monteiro et al. (2016)]. Therefore, probabilistic approaches become imperative for accurate risk-based decision-making strategies. Many researchers have used reliability frameworks over the last two decades as they are versatile, allow the propagation of uncertainties efficiently, and can take advantage of experimental studies, observations, and theoretical aspects [e.g., Frangopol et al. (2008); Strauss et al. (2013); Thanapol et al. (2016), Gong and Frangopol (2019)]. For instance, the traffic flow prediction and its physical model are crucial components for an accurate structural reliability assessment. Many studies have adopted either extreme value analyses [e.g., O'Connor and O'Brien (2005); Caprani and O'Brien (2006); Enright and O'Brien (2013)] or peak-over-threshold methods [e.g., Zhou et al. (2016); Nesterova et al. (2020)] to determine the maximum traffic load on bridges. However, uncertainties on the vehicular flows can cause large variability and, if ignored, could lead to non-conservative solutions. Recent developments of accurate site traffic measurements (e.g., weight-in-motion, WIM) have provided databases and statistical models of the traffic loading demand [e.g., Chan et al. (2005); Guo et al. (2012)] to obtain an adequate estimate of the traffic flow prediction. It is then essential to have a realistic approach for the traffic generation, which should accurately model off- and on-peak extreme values.

The structural capacity is also related to degrading phenomena over time, i.e., corrosion [e.g., Akyama et al. (2011); Akyama and Frangopol (2014)]. Typically, chlorides penetrate through the concrete and de-passivate the layer of film protecting the steel reinforcement [e.g., Chen et al. (2018)]. Such a de-passivation leads to an expansion of the steel volume due to the rust, which produces localised tensile stresses resulting in cracking of the concrete cover and the un-effective concrete core, reducing the steel and concrete mechanical properties [e.g., Zhong et al. (2010); Di Sarno and Pugliese (2020)]. Such phenomena are time- and case-study-dependent and require a wide range of relevant random parameters [e.g., Ghosh and Sood (2016)]. Therefore, deterministic assumptions are not accurate to simulate the random progress of the corrosion initiation, propagation, and deterioration and have the drawback of being unable to incorporate data from inspections [Calvert et al. (2020)].

The weather is another critical aspect influencing the corrosion damage. In particular, the increasing differential between the minimum and maximum temperatures is causing a significant negative impact on RC components by reducing the occurrence time of the corrosion initiation and increasing the corrosion rate. This topic has been scarcely considered to predict the time initiation, propagation and deterioration of corrosion in RC structures [e.g., Stewart et al. (2011); De Larrard et al. (2014)]. Many existing RC bridges are subjected to extreme seasonal temperatures and relative humidity variability. As a result, current applications and numerical analyses should account for such effects that include time-dependent climate-related actions.

This study presents a comprehensive probabilistic time-dependent reliability framework that combines the increasing traffic loading and the exposure to non-uniform corrosion for existing RC bridges, using a holistic approach. Such a holistic approach is versatile and can

be used for different and broader frameworks, i.e., earthquakes and life-cycle cost assessment [e.g., Shekhar and Ghosh (2020)]. A refined finite element (FE) model of an existing thirteen-bay RC bridge is implemented in OpenSees [McKenna et al. (2000)]. A probabilistic model for generating a realistic traffic flow, built upon the previous literature, is provided and incorporated in the FE model. The method uses an available WIM database from the literature, which is not specific for this case, but it is deemed accurate and reliable for demonstrating the proposed procedure. Instead, the traffic flow prediction is based on realistic data acquired from the national highway database (www.autostrade.it).

The time-dependent decrease in the mechanical properties of materials for the RC bridge is simulated through the spatially variable pitting corrosion. Given the long extension of bridges and viaducts, time to corrosion initiation, propagation and deterioration may occur randomly across RC bridges; such uncertainty can be accounted for considering possible spatial correlations. The pitting factor and the time to corrosion initiation are the two parameters with the highest uncertainty and are considered statistically independent. This study includes two spatial correlations for both parameters: (a) complete and (b) zero correlation.

Experimental studies are used to develop the probabilistic model through the cracking initiation, pitting factor, severe cracking, and spalling of the concrete cover. Such statistical distributions can be used as a benchmark for practical applications and are versatile to be applied for RC components exposed to various highly corrosive environments (e.g., splash marine, de-icing salts, atmospheric).

The minimum and maximum annual temperatures are collected from local meteorological stations to account for the weather-related features and their effects on corrosion initiation. Such data are fitted through statistical distributions and used as an upper and lower bound to estimate the environmental factor. Thus, a comparison with the existing mathematical distribution of the environmental factor for atmospheric corrosion is carried out to evaluate the occurrence time of the corrosion initiation.

Monte Carlo simulations are performed at intervals of 10 years to compute the structural demands (e.g., axial, shear and bending) for each bridge pier (and, more in general, all bridge components). Such a simulation approach is consistent with Arismendi et al. (2021). For a proper structural reliability assessment, the capacity parameters are divided into two groups: (a) flexural failure or ductile mechanisms and (b) shear failure or brittle mechanisms. The ductile mechanisms are evaluated through the three-dimensional interaction surface of RC cross-sections (columns, intermediate beams and cap-beams of the piers) subjected to biaxial bending moment and axial loading. Such a three-dimensional surface model is employed in an advanced software platform for structural analysis, which may account for the effects of corrosion on the constitutive materials of steel and concrete. Conversely, due to the complexity and the lack of experimental studies on the shear failure of RC components subjected to corrosion, a response surface approach is used to obtain the capacity of brittle mechanisms of aged RC sections. The surrogate models of the shear capacity of corroded RC bridge elements are developed using the results obtained from the modified compression field theory [Vecchio and Collins (1986)].

Finally, the safety margin and the associated reliability indices are computed over time. Such values are then compared against technical standard thresholds to define when the bridge is no longer compliant with current limits and requires maintenance interventions.

2. DESCRIPTION OF THE FE RC BRIDGE MODEL

An existing continuous RC bridge located in Italy (Rio Torto bridge) was used as a testbed for the present numerical study. The RC bridge, built in the 1960s, represents an essential component of the transportation network for the Italian highways (connecting Bologna to Florence, as shown in Figure 1).

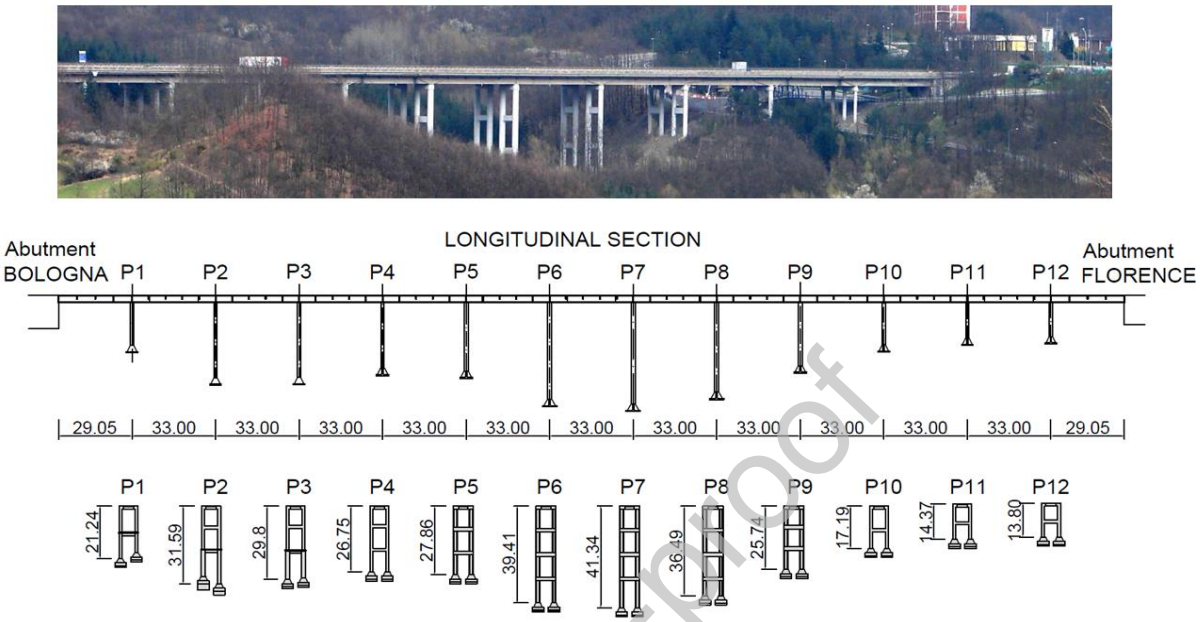

Figure 1. RC Bridge layout view [*after* De Risi et al. (2017)].

The thirteen-bay deck is supported by twelve portal frames that comprise solid (labelled as P1, P2, P3, P4, P10, P11 and P12 in Figure 1) and hollow (labelled as P5, P6, P7, P8, and P9 in Figure 1) circular columns with diameters varying between 1200mm and 1600mm. Such portal frames include two circular piers connected by intermediate beams with different sections and cap-beams at the top. The RC bridge height varies between 13.8m, close to the abutments, and 41m at its centre. The RC slab deck has a Π-shape (total depth equal to 2.75m, Figure 2) connected to the portal frame through dowels (shear connections) represented by two steel bars inserted into the concrete.

The solid piers with a 1200mm and 1600mm diameter are reinforced with 16ϕ20mm and 20ϕ20mm smooth rebars, respectively, with a transverse spiral hook ϕ6mm with 140mm spacing. On the other hand, the hollow piers have an internal and external diameter equal to 1000mm and 1600mm with two reinforcing configurations: (a) 24ϕ20mm external and 14ϕ16mm internal, (b) 20ϕ20mm external and 14ϕ16mm. The transversal reinforcement consists of a spiral hook ϕ6mm with 150mm spacing.

Rectangular (depth varying between 1200 and 1500 mm) and T-shape cross-sections were used as intermediate beams; the longitudinal reinforcements include ϕ24 and ϕ20 steel bars, while transversal reinforcement consists of ϕ8 steel bars with a spacing of 200 mm. The cap-beams have a rectangular cross-section at the top of the pier and present a U-shaped section at the centre. Such beams are reinforced mainly with ϕ18 longitudinal bars and ϕ8 transversal reinforcement with 200mm spacing (Figure 3).

Figure 2. The layout of the deck (Units in *mm*)

Experimental tests were carried out to characterise the concrete and steel reinforcement material properties. Compressive tests on 15x15x15 cm^3 cube specimens were conducted to define the concrete strength of the bridge portal frames, while tensile tests were used to determine the steel reinforcement properties [Abbiati et al. (2015)]. Probabilistic distributions are then used to account for uncertainties. Mainly, the concrete class is simulated through a lognormal distribution with a mean resistance of 26 MPa (defined by the experimental campaign) and a coefficient of variation (COV) equal to 0.15 [Jalyer et al. (2015)]. The class of steel used corresponds to a mean strength of 360 MPa, which complies with the experimental tests [Abbiati et al. (2015)] and past studies available in the literature [e.g., Verderame et al. (2001)]. A lognormal distribution is used for simulating the constitutive model of steel reinforcement with a COV of 0.08. Table 1 shows the random parameters of the mechanical and geometrical properties of the RC bridge.

Table 1. Statistical mechanical and geometrical properties of RC components (Keys: *LN* – lognormal distribution, μ and *COV* for the lognormal distribution are the mean and the coefficient of variation of the associated normal distribution)

Description	Parameter	Distribution (μ, COV)	Units
Concrete Compressive strength	f_c	LN (26, 0.15)	MPa
Yielding stress of steel bars	f_y	LN (360, 0.08)	MPa
Elastic modulus of steel bars	E_s	LN (207000, 0.05)	MPa
Cover	c	LN (40, 0.20)	mm
Diameter of sound steel bars	D_0	LN (variable, 0.035)	mm

A refined FE model of the RC bridge was employed in an advanced software platform for structural analysis (OpenSees). An elastic beam-column with an equivalent section, in terms of second moments of inertia, of the original box-girder shape was used to model the bridge deck (Table 2), while force beam elements [Spacone et al. (1996a -1996b)] with five integration points (Gauss-Lobatto) were utilised to simulate the behaviour of the cap-beams, intermediate beams, and piers.

Table 2. Deck characteristics [*after* Paolacci et al. (2014)]. (*Keynote: J – Polar moment of inertia, I_y and I_z – Moment of inertia with respect to the local axis of the bridge deck*)

Area (m^4)	J (m^4)	I_y (m^4)	I_z (m^4)

4.66	0.13	51.87	3.47

Each integration point is characterised by nonlinear fibres, behaving according to the stress-strain models of concrete (Popovics concrete model, named Concrete04 in OpenSees) and steel reinforcement (Steel Menegotto-Pinto model, named Steel02 in OpenSees). The Popovics model allows to define the tensile behaviour of the concrete, which is relevant when corrosion induces the complete loss of steel reinforcement bars in the RC cross-section and the model does not produce global instability or convergence issues. The steel material is defined according to the parameters included in Di Sarno et al. (2021).

The deck weight is about 170kN/m; this produces a vertical load on each pier between 4,900kN and 5,600kN. The piers are fixed at the base (as the RC bridge lies on rocks), and the fixed-end rotation is modelled with a zero-length section, whereas the Hysteretic model is used to simulate the strain penetration of steel reinforcement. Such a hysteretic model in OpenSees was calibrated through the experimental tests conducted on smooth rebars by Fabbrocino et al. (2005) and Verderame et al. (2009), among the others. The core concrete properties are implemented in the zero-length section as stress-displacement (d_{cc}); The latter is computed by multiplying the concrete core strains (ε_{cc} the strain at the peak of the confined concrete, ε_{ccu} the ultimate strain of the confined concrete) ten times the mean longitudinal diameter (D_l) in the bridge pier section according to Fabbrocino et al. (2005) (i.e., $d_{cc} = \varepsilon_{cc} x 10 D_l$). The shear connection (dowels) between the deck and the portal frame is simulated with an equal DOF (degree of freedom) in the transversal direction, whereas the master node is represented by the centroid of the equivalent elastic beam deck. Finally, the bridge was pinned at both abutments allowing the rotation in the three global directions.

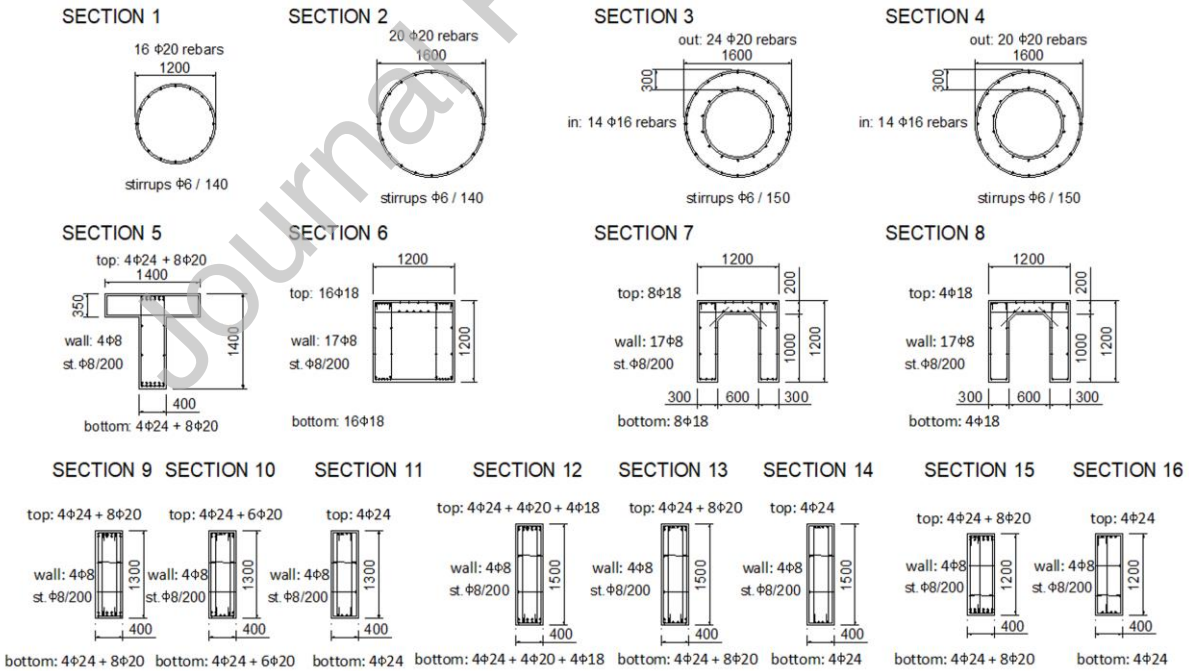

Figure 3. RC Cross-Section of Piers and Beams (Units in mm)

Based on the mean values of the model parameters illustrated in Table 1, the modal analysis shows that the first three modes exhibit the following period of vibration: T_1 = 1.34 sec, T_2 = 1.10 sec and T_3= 0.81sec.

3. CORROSION MODEL

Typically, a thin layer of iron oxide (Fe_2O_3) film protects steel reinforcement bars from the high alkalinity of the concrete. However, high chloride contents in the cement paste and external factors (i.e., de-icing salts, marine splash) de-passivate this layer, activating the corrosion process. Corrosion of steel reinforcement is one of the most critical factors for the durability performance of RC structures over time. Due to the many corrosion-related uncertainties, it is common to characterise the corrosion process into three subcategories: corrosion initiation (t_{ini}), propagation (t_{prop}), and deterioration (t_{det}).

3.1 CORROSION INITIATION

The most adopted probabilistic model for corrosion initiation is the DuraCrete (2000) model, which refers to the diffusion process of the chlorides defined by Fick's second law.

$$C(x = c, t) = C_{S0}\left[1 - erf\left(\frac{c}{2\sqrt{k_e k_c k_t \mathrm{D}_{app} t}}\right)\right] \quad (1)$$

where x is the chloride penetration depth, D_{app} is the apparent coefficient of the chloride diffusion ($D_{app} = D_{Cl}\left(\frac{t_0}{t}\right)^{n_{cl}}$, D_{Cl} is the chloride migration coefficient and t_0 is the reference time, which is commonly equal to 28 days), C_{S0} is the chloride content on the concrete surface, c is the concrete cover, t is the time, k_e is the environmental coefficient accounting for the temperature, k_c is the curing time coefficient, k_t is the correction coefficient for the test method, n_{cl} is the age factor and $erf(\cdot)$ is the Gauss error function.

Such a probabilistic model assumes that the initial value of the chloride contents in the cement paste is equal to zero, and the corrosion initiation occurs when the chloride concentration on the steel bars reaches a critical value $C(x = c, t) = C_{crit}$. Once the chloride content is at its critical value, the time t is identified with corrosion initiation and denoted by t_{init}. As a consequence, solving Eq. (1) for the $t = t_{init}$:

$$t_{init} = X_1\left\{\frac{c^2}{4k_e k_c k_t D_{Cl} t_0^{n_{cl}}}\left[erf^{-1}\left(1 - \frac{C_{crit}}{C_{S0}}\right)\right]^{-2}\right\}^{\frac{1}{1-n_{cl}}} \quad (2)$$

where X_1 represents the parameter to account for the model uncertainty related to the Fick's second law.

The corrosion process depends on the location of a structure. There are four subcategories characterising the corrosion zone [DuraCrete (2000)]: (a) submerged, (b) tidal, (c) splash, and (d) atmospheric. Each category produces different times to corrosion initiation due to the change in the model parameters.

The Rio Torto bridge is located close to water streams, which are the primary sources of dissolved airborne marine chlorides. Therefore, the bridge falls into the category of atmospheric corrosion (d); Table A1 shows the model parameters in Eq. (2).

3.2 ENVIRONMENTAL COEFFICIENT

Atmospheric corrosion is a complex process that depends on several environmental factors, i.e., temperature, and is the primary cause of corrosion in steel reinforcement of bridges. The

effects of global warming and, in turn, climate change are increasing the likelihood of corrosion in RC structures because of the growth of the corrosion rate. As a result, the impact of climate change on the performance of RC structures is substantial. The environmental factor is expressed as a function of the temperature as follows:

$$k_e = \exp\left[b_e\left(\frac{1}{T_{ref}} - \frac{1}{T_{real}}\right)\right] \quad (3)$$

where b_e is a regression parameter defined by a truncated normal distribution, with mean 4,800[K] and standard deviation 700[K], included in the interval (2,130 ; 5,500) [K]; T_{ref} (also termed "room temperature") is the reference temperature, commonly equal to 293.15 [K]; T_{real} is the real temperature of RC components or the ambient air temperature. Equation (3) is used to compare the environmental coefficient proposed by DuraCrete (2000) and the value obtained from the actual temperature measured in the sample bridge location. The Italian database (*www.ilmeteo.it*) for the meteorological station of Borgo Panigale is used to collect the minimum and maximum mean temperature for the time span 1960-2020.

The generalised extreme value distribution (GEV) with its three parameters (location parameter μ_G, scale parameter σ_G, and shape parameter k_G) seems to adequately fit the empirical cumulative density function (ECDF) both for the minimum and the maximum temperatures (Figure 4). Such statistical distributions can be used as lower (T_{min}) and upper (T_{max}) boundaries to calculate the environmental coefficient in Eq. (3). Performing a Montecarlo simulation across 50,000 samples (Figure 5), the environmental factor can be accurately estimated by a gamma distribution having a and b parameters equal to 3.79 and 0.23, respectively.

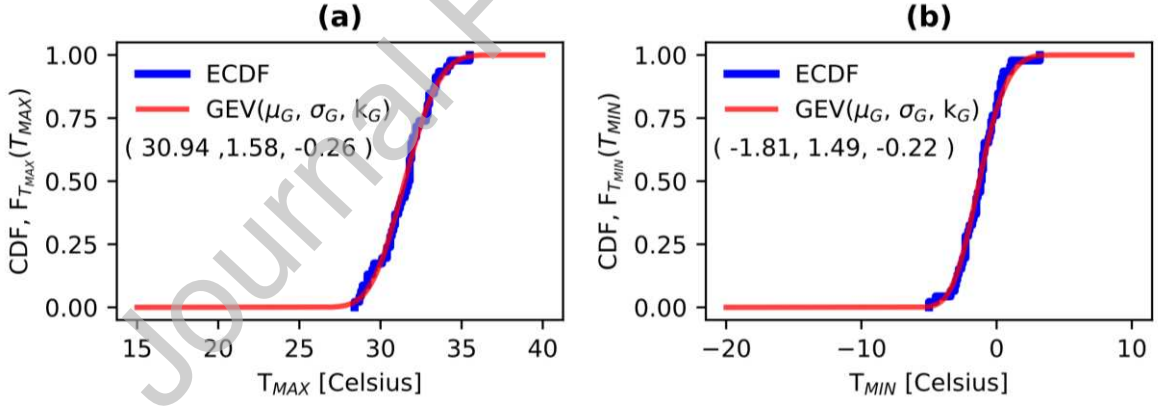

Figure 4. Probabilistic distribution for (a) T_{max} and (b) T_{min} (Borgo Panigale Station)

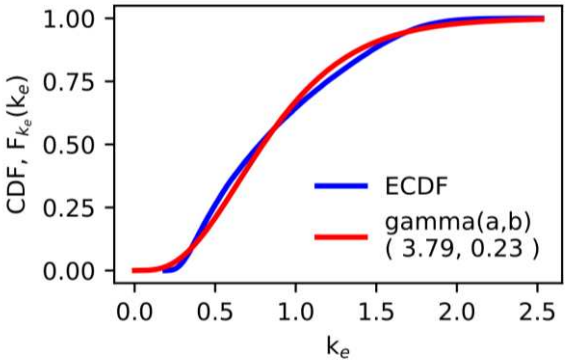

Figure 5. Probabilistic distribution fitting of the environmental factor

Based on the assumption of the model parameters given by DuraCrete (2000), the actual values of the environmental factor and a lifetime of 100 years according to the EN-1992 (2004), the comparison of the time to corrosion initiation for the Rio Torto bridge is presented (Figure 6a and 6b). Corrosion initiation is estimated by running a Montecarlo over 100,000 samples.

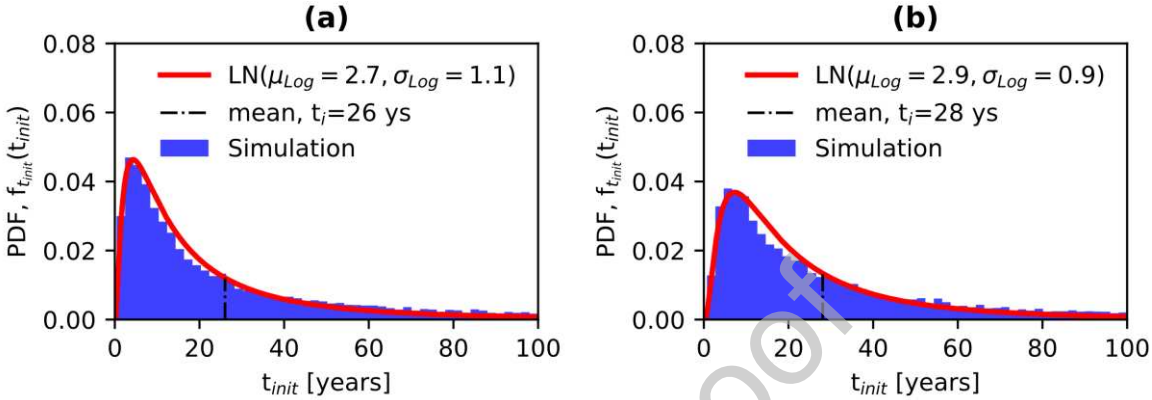

Figure 6. Time initiation of corrosion. (a) k_e from the temperature data, (b) k_e from Duracrete (2000). (*keynote*: μ_{Log} and σ_{Log} are the mean and standard deviation of logarithmic values, respectively)

A lognormal distribution (with its two parameters μ_{Log} and σ_{Log}, the mean and standard deviation of logarithmic values, respectively) appears to be a reasonable estimate of the numerical simulation for the time to corrosion initiation. The comparison between the numerical simulations based on the value of k_e calculated using the minimum and maximum temperature cycles and the value of k_e proposed by DuraCrete (2000) shows that corrosion initiation decreases from 28 to 26 years. Although it seems to be a slight difference, such a reduction can be detrimental for a long-time exposure of RC bridges to the atmospheric corrosion by decreasing the time-to-severe cracking and the following time-to-spalling of the concrete cover.

3.3 CRACKING INITIATION

When the localised tensile stress, induced by the expansion of the rust products, reaches the critical value of the concrete tensile strength, crack initiates. Then, the corrosion rate becomes the critical factor for the reinforcing steel damage and deterioration. The end of the corrosion propagation phase (for the diffusion of chlorides in the concrete after the time to corrosion initiation) coincides with the onset of the cracking initiation (time for crack initiation, t_{cr}), which can be expressed by:

$$p(t) = R \int_{t_{init}}^{t_{cr}-t_{init}=t_{prop}} r_i(t)dt \quad (4)$$

where $p(t)$ is the pit depth with time, R is the pitting factor defined as the ratio between the maximum pit depth (p_{max}) and the mean pit depth (p_{mean}), and $r_i(t)$ is the corrosion rate. The corrosion rate is namely expressed in mm/year and is a function of the time-dependent current density ($i_{corr}(t) = 0.85\, i_{corr,0}(t=0){t_{prop}}^{-0.29}$):

$$r_i(t)(mm/y) = 0.0116 i_{corr}(t) \quad (5)$$

To investigate the critical pitting depth $p_{crit}(t = t_{cr})$, Alonso et al. (1998) conducted an experimental campaign to evaluate the amount of corrosion penetration (x_0) to trigger cracking in the concrete, assuming uniform corrosion. Such experimental results are herein taken to determine the plausible probabilistic distribution for the cover cracking initiation. It is assumed that the variance of residuals of the regression model is constant (homoscedastic model), while the logarithmic regression is used to interpolate the data (Figure 7a). The contribution of the concrete tensile strength is neglected at this point. This assumption also complies with the investigation by Vidal et al. (2004). The critical pit depth can then be expressed by a lognormal distribution with a mean computed through the equation in Figure 7a and a constant standard deviation equal to 0.18, multiplied for the corresponding pitting factor *R*.

Likewise, the pitting factor *R* is relevant for assessing the residual capacity of RC components as it defines the critical pit depth along reinforcing bars. Experimental studies were carried in the literature to study the realistic range of such a factor, but only few focussed on the diameters of interest in the framework assessment of typical RC components [e.g., Rodriguez et al. (1997); Torres-Acosta et al. (2003); Yu et al. (2015)]. Therefore, the experimental campaigns with steel bar diameters (12mm, 13mm, and 16mm) complying with existing RC structures were collected to identify the statistical distribution of the pitting factor.

The generalised extreme value seems (Figure 7b) to adequately fit the R-values obtained from short- and long-term experimental studies, which is compliant with some studies available in the literature [e.g., Stewart and Al-Harthy (2008)].

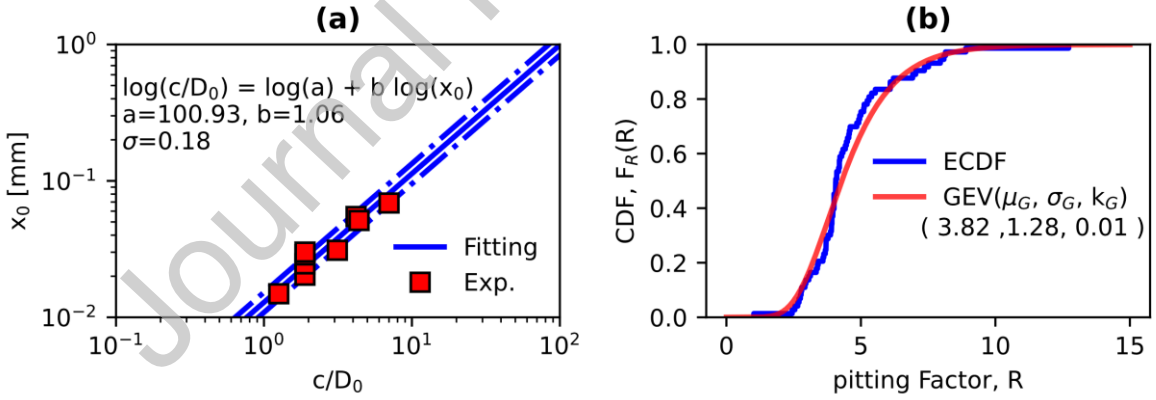

Figure 7. (a) Critical pit depth and (b) Pitting Factor statistical distributions

Once the parameters of the critical depth and the pitting factor are defined, the Eq. (4) can be solved for t_{cr}, which represents the mean of a lognormal distribution whose standard deviation (0.53μ) is taken from the results of Thoft-Christensen (2000):

$$t_{cr} = t_{init} + \left[\frac{p_{crit} = (x_0 R)}{0.0139\, R\, i_{corr}(t = 0)}\right]^{1.41} \quad (6)$$

The general form of Eq. (6) was introduced by Cui et al. (2018).

3.4 SEVERE CRACKING AND CONCRETE SPALLING

The progress of corrosion leads to two specific aspects: severe cracking and spalling of the concrete cover. The first one is associated with a critical crack width (w_{sc}), which is herein provided as a uniform distribution with extreme values 0.2-0.3 mm (Figure 8). Conversely, the crack width for the concrete cover spalling (w_{sp}) is not specified in technical codes, but existing studies [e.g., Vidal et al. (2004); Duracrete (2000)] suggest assuming a value of 1.0mm. However, the experimental campaign by Rodriguez et al. (1996) indicates that such a value is quite conservative. As a result, the width crack leading to spalling of the concrete cover, based on experimental evidence, is herein expressed by a lognormal distribution and used as a random input variable (Figure 8).

Thus, the equations proposed by Cui et al. (2018) can be used for characterising the time-to-severe cracking and -spalling:

$$p_{sev}(t) = p_{cr}(t) + R(t)\int_{t_{init}}^{t_{sev}-t_{cr}=t_{det}} r_i(t)dt \tag{7a}$$

$$p_{spa}(t) = p_{sev}(t) + R(t)\int_{t_{init}}^{t_{spa}-t_{sev}=t_{det}} r_i(t)dt \tag{7b}$$

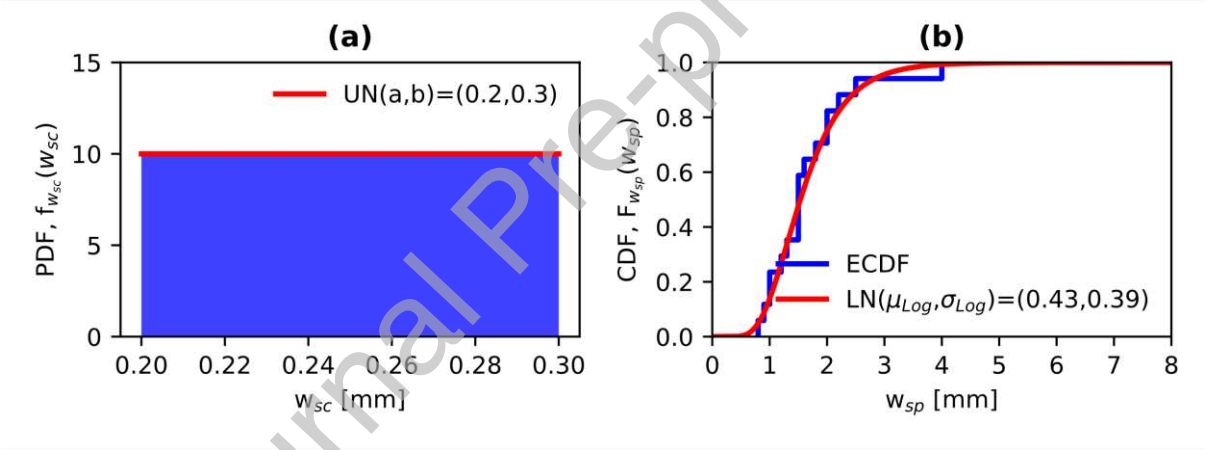

Figure 8. (a) Severe crack width (w_{sc}) and (b) crack width for spalling of concrete cover (w_{sp}). (*keynote*: μ_{Log} *and* σ_{Log} are the mean and standard deviation of logarithmic values, respectively)

However, such parameters depend upon the area loss of steel reinforcement due to pitting corrosion. To evaluate the reduction of the steel area, Vidal et al. (2004) proposed a correlation between the crack width and the area loss based on an experimental campaign of corroded RC beams:

$$\mathrm{w(t)} = 0.0575[\Delta A_{i+1} - \Delta A_{\mathrm{CR}}] \tag{8}$$

where $\Delta A_{i+1} = A_0 - A_{corr}(t)$ (A_0 and $A_{corr}(t)$, area of uncorroded and corroded steel, respectively) is the steel area loss at the time t, $\Delta A_{\mathrm{CR}} = A_0 - A_{CR}$ (A_{CR} is the remaining area after cracking initiation) is the steel area loss at the cracking initiation and, w is the crack width.

Once the value of $A_{corr}(t)$ is obtained from Eq. (8), it is then possible to compute the pit depth at either cover severe cracking or cover spalling by solving the Eq. (7a and 7b).

4. NUMERICAL PROCEDURE FOR THE DETERIORATION MODEL

In this section, the description of the numerical procedure for the deterioration model in the FE analysis is presented. The flowchart of the proposed procedure for the corrosion model is shown in Appendix A, Figure A1.

4.1 DETERIORATING FINITE ELEMENT MODEL

Once the statistical distributions of each parameter characterising the corrosion stages are defined, the deterioration can be applied to the FE model of the bridge.

First, the mechanical and geometrical properties of the constitutive materials and the RC cross-sections are generated to build the model in OpeenSees. Then, the time to corrosion initiation of each portal frame is simulated using Eq. (2) with the random samples generated according to the parameters defined in Table A1. The GEV in Figure 7b yields the pitting factor *R* that can be either constant or variable among the piers depending on the correlation structure. The concrete cover-to-diameter ratio allows to model the critical pitting depth with a lognormal distribution (Figure 7a). These two parameters, pitting factor (*R*) and critical pitting depth (p_{crit}), are independent of the corrosion initiation. Hence, a lognormal distribution with a mean equal to Eq. (6) gives the time to cracking initiation.

The model of Val and Melchers (1997) can then be used to calculate the remaining steel reinforcement area due to the pitting corrosion (Figure 9 and Eq. (9), (10) and (11)).

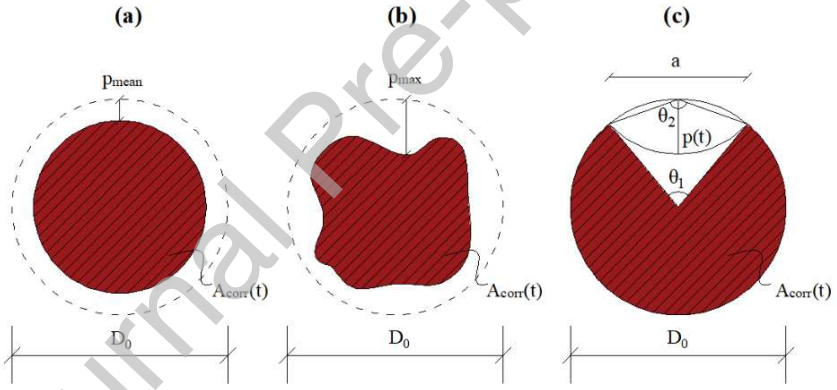

Figure 9. (a) Uniform corrosion, (b) pitting corrosion and (c) Val and Melchers' model (*keynote*: p_{mean} -average pit depth, p_{max} – max pit depth, D_0 – diameter of the sound steel)

$$A_{corr}(t) = \begin{cases} \frac{\pi d_0^2}{4} - (A_1 + A_2) & p(t) \le \frac{D_0}{\sqrt{2}} \\ A_1 + A_2 & \frac{D_0}{\sqrt{2}} < p(t) \le D_0 \\ 0 & p(t) \ge D_0 \end{cases} \quad (9)$$

$$A_1 = \frac{1}{2}\left[\theta_1 \left(\frac{D_0}{2}\right)^2 - a\left|\frac{d_0}{2} - \frac{p(t)^2}{D_0}\right|\right],\ A_2 = \frac{1}{2}\left[\theta_2 p(t)^2 - a\frac{p(t)^2}{D_0}\right] \quad (10)$$

$$\theta_1 = 2\arcsin\left(\frac{2a}{D_0}\right),\ \theta_2 = 2\arcsin\left(\frac{a}{p(t)}\right),\ a = 2p(t)\sqrt{1-\left(\frac{p(t)}{D_0}\right)^2} \quad (11)$$

After the cracking initiation, the statistical distributions in Figures 8a and 8b yield the crack width for severe cracking (w_{sc}) and spalling of the concrete cover (w_{sp}). Such values are incorporated into Eq. (8) for $A_{i+1} = A_{corr}(t)$ (Figures 9). A numerical method is used to solve Eq. (9), (10) and (11) for the pitting depth *p(t)*.

Once the values of $p_{sev}(t)$ and $p_{spa}(t)$ in Eq. (7a) and (7b) are determined, such formulations can be solved for the time parameter, which represents the mean of a lognormal distribution with a standard deviation equal to 0.53μ. The pitting factor is simulated differently for the cracking initiation, severe cracking and spalling of the concrete cover, such that:

$$R(spalling) > R(severe\ cracking) > R(cracking\ initiation) \quad (12)$$

When the cracking width reaches the critical values of the spalling of the concrete cover, this latter does not contribute any longer to the RC cross-section capacity and is removed from the cross-section. Table 3 summarises the statistical distributions for the crack width and corrosion phases.

Table 3. Statistical distributions for crack width and corrosion phases (*keynotes*: μ and σ for the lognormal distribution are the mean and the standard deviation of the associated normal distribution)

Description	Distribution		
Cracking Initiation	Lognormal	Mean (μ) [mm] $p_{crit} = e^{-\left[\frac{\ln(c/D_0)-4.61}{1.06}\right]}$	Standard Deviation (σ) [mm] 0.18
Severe cracking	Uniform	Lower Bound [mm] 0.2	Upper Bound [mm] 0.3
Spalling	Lognormal	Mean (μ) [mm] 1.66	Standard Deviation (σ) [mm] 0.68
		Mean (μ) [year]	Standard Deviation (σ) [year]
Time to cracking initiation	Lognormal	Eq. (6)	0.53 μ
Time to severe cracking	Lognormal	Eq. (7a)	0.53 μ
Time to cover spalling	Lognormal	Eq. (7b)	0.53 μ

At each time step, the corrosion percentage rate (*CR*) is calculated by means of the area loss of the steel reinforcement bars, as follows:

$$CR(t)[\%] = \frac{A_0 - A_{corr}(t)}{A_0} \times 100 \quad (13)$$

Such a loss of steel reinforcement area has significant effects on the strength and ductility of steel bars. In particular, the strength reduction can be calculated by assuming a linear relationship between the yield stress (f_y^{corr} and f_y, yielding stress with and without corrosion, respectively) and the corrosion percentage rate [e.g., Zhang et al. (1995)]:

$$f_y^{corr} = f_y(1 - 0.01CR[\%]) \quad (14)$$

An exponential relationship can be used to compute the ductility decrease through the ultimate strain (ε_{su}^{corr} and ε_{su}, ultimate strain with and without corrosion, respectively) [e.g., Imperatore et al. (2017)]:

$$\varepsilon_{su}^{corr} = \varepsilon_{su} e^{-0.055 CR[\%]} \tag{15}$$

When steel bars start rusting, there is an expansion of the volume of steel filling the pores in the concrete. This latter produces local tensile stresses, typically within the concrete cover and the un-effective concrete core, that reduces the compressive strength of the un-confined and confined concrete. The reduction factor (RF) can be calculated as follows [e.g., Coronelli and Gambarova (2004)]:

$$f_c^{corr} = RF\, f_c \qquad RF = \frac{1}{1 + 0.1\frac{w(t) n_{bars}}{L \varepsilon_{c0}}} \tag{16}$$

where f_c^{corr} and f_c are the compressive strengths with and without corrosion, n_{bars} is the number of steel bars on the side of exposure, L ($L = \pi D_0$ for circular columns) is the dimension on the side of exposure, and ε_{c0} is the strain at the peak of the un-confined compressive strength.

According to Di Sarno and Pugliese (2020), the effects of corrosion on the compressive strength are also included in the un-effective core concrete for a length twice the mean diameter of the steel reinforcement bars (Figure 10). On the other hand, the effective concrete core is not affected by the corrosion effects [e.g., Andiseh et al. (2019)]. These two observations lead to the following reduction of the confined compressive strength:

$$f_{cc}^{corr} = \frac{A_{UN}\, RF\, f_{cc} + A_{EF}.f_{cc}}{A_{UN} + A_{EF}} \tag{17}$$

where f_{cc} is the un-corroded compressive strength of the confined concrete (computed according to Razvi and Saatcioglu (1999), f_{cc}^{corr} is the corroded compressive strength of the confined concrete, A_{UN} and A_{EF} are the area of the un-effective and effective concrete core, respectively (Figure 10).

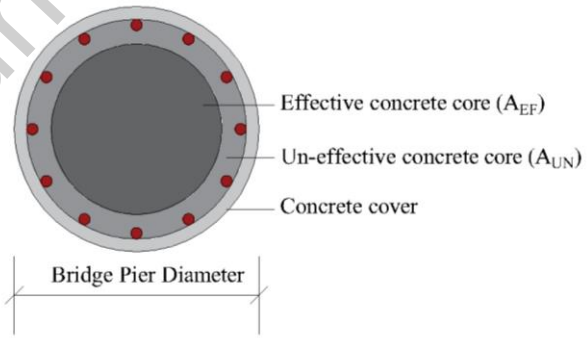

Figure 10. RC cross-section

4.2 SIMULATION-BASED APPROACH

Two statistical independent univariate homogenous random fields are defined for the pitting factor (R) and the time to corrosion initiation (t_{ini}). Two limit cases are considered in this study: (a) the distance between piers is larger than a limit value implying no correlation (hereinafter indicated as $\rho = 0$), and (b) the distance between piers is smaller than a limit value implying complete correlation (hereinafter indicated as $\rho = 1$). The limit value of pier inter-distances cannot be determined in this study due to the lack of systematic testing on all

the piers to calibrate a proper correlation model. The reality will lie in between the two extreme cases examined herein.

5. RELIABILITY ASSESSMENT

The time-varying reliability, herein considered at a component level, is defined as the probability that an RC element does not exceed a specific limit state for a given time. Such a limit commonly refers to the performance function (safety margin) denoted by G(t). The limit state function is expressed as the difference between the capacity C(t) and the demand D(t) of the RC component.

$$G(t) = C(t) - D(t) \tag{18}$$

In the present study, the performance function is divided into ductile and brittle mechanisms; the first ones are described by the three-dimensional interaction domain of the biaxial bending moment and axial loading, while the second ones refer to the shear strength of RC cross-sections. When the function G(t) < 0, the RC component fails.

One of the major issues when dealing with corrosion, especially in the long-term ($t \geq 90{,}100\ years$), is that the FE may enter the region of global instability, meaning that one or more components are no longer able to withstand the structural loadings. Such an observation refers to the significant effects of corrosion on both the mechanical and geometrical properties of the constitutive materials and the increasing traffic demand, which induce very high forces in RC elements compared to their actual capacity. The latter aspect conditions the limit state function and can produce unreliable results. Therefore, the analyses with global instability (due to incompatible element forces) are treated as collapse scenarios. In the following, according to Jalayer (2003), $\bar{C}$ is used to indicate the number of non-collapse cases, C refers to the number of collapse cases and N_{sim} is the number of total simulations.

Specifically, Shome (1999) provided a three-parameter distribution to solve such an issue for seismic evaluation assessments. For the general reliability case, it can be changed as follows:

$$P_{f,TOT}(t) = P(G(t) < 0|\bar{C})\frac{\bar{C}}{N_{sim}} + P(G(t) < 0|C)\frac{C}{N_{sim}} \tag{19}$$

where the probability $P(G(t) < 0|C)$ of exceeding any specific limit given collapse is equal to 1. Eq. (19) can be definitely written in the form:

$$P_{f,TOT}(t) = P(G(t) < 0|\bar{C})\frac{\bar{C}}{N_{sim}} + \frac{C}{N_{sim}} \tag{20}$$

Finally, the reliability index (β), which is a measure of the structural safety, can be calculated as function of the failure probability:

$$\beta(t) = -\phi^{-1}\left(P_{f,TOT}\right) \tag{21}$$

In the above equation, Φ indicates the standard normal cumulative distribution function.

5.1 MONTE CARLO SIMULATION

The number of simulations is derived using the following equations [e.g., Ang and Tang (2007)]:

$$COV = \frac{\sqrt{\frac{p_f(1-p_f)}{N_{sim}}}}{p_f} \qquad N_{sim} = \frac{(1-p_f)}{p_f COV^2} \tag{22}$$

where p_f is probability of failure, N_{sim} the total number of simulations, and COV is the coefficient of variation of the estimation. Assuming that the expected value of the failure probability is equal to the reliability level for a lifetime of 100 years ($\pi = 7.2x10^{-5}$) and COV to 40%, the optimal number of simulations is 86,800. In this study, 100,000 simulations are performed at each time interval.

5.2 FAILURE MECHANISMS

As mentioned previously, two failure mechanisms are considered for the reliability assessment of the Rio Torto bridge: (a) ductile mechanisms (herein referred to as flexural capacity of RC cross-sections of each portal frame) and (b) brittle mechanisms (herein referred to as shear capacity of RC cross-sections of each portal frame).

Based on the dual failure mechanisms, the concept of cut-set [e.g., Ditlevsen and Masden (1996)] is adopted to evaluate the reliability of portal frames ($P_{f,SYSTEM}$) composing the RC bridge. Such a cut-set method allows to define the failure probability of the global system as follows:

$$P_{f,SYSTEM}(t) = max_{i=1}^{N_{mech}} max_{j=1}^{N_{elem}} P_{f,TOT_{ji}}(t) \tag{23}$$

where N_{mech} is the number of failure mechanisms, N_{elem} is the number of elements of the considered portal frame.

The Eq. (23) can also be defined in terms of reliability index (β):

$$\beta(t) = min_{i=1}^{N_{mech}} min_{j=1}^{N_{elem}} \beta_{ji}(t) \tag{24}$$

5.2.1 DUCTILE MECHANISM: FLEXURAL CAPACITY OF CORRODED RC COMPONENTS

The three-dimensional interaction domain of the axial loading (P_x, x refers to the axis of the element) and biaxial moment (M_y and M_z, where y and z refer to the RC cross-section axes) is herein adopted to evaluate the flexural capacity of each RC section composing the sample bridge. The P_x - M_y - M_z point determines the demand in the 3D-domain whereas the flexural capacity is calculated drawing a vector from the origin of the 2D-domain M_y - M_z (plane with constant axial loading) that points to the demand and extends to the limit surface with the same angle (α) (Figures 11).

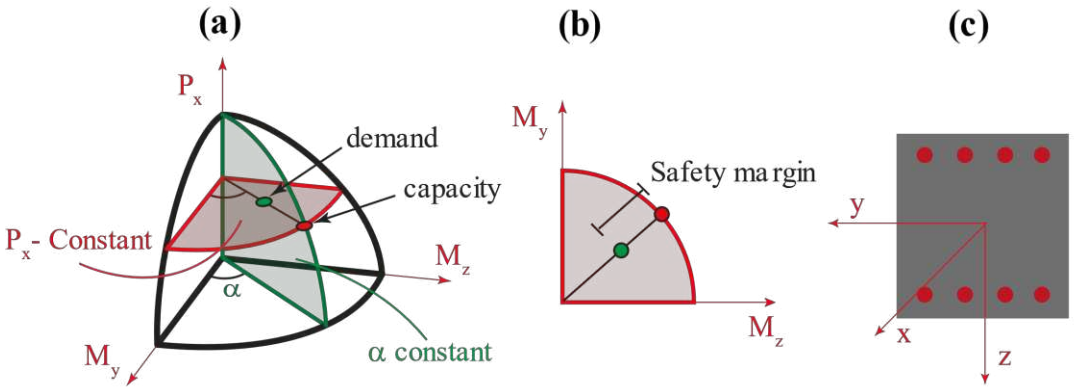

Figure 11. (a) 3D-Interaction domain, (b) Safety Margin and (c) RC cross-section local axes

According to resistance formulation (5.39) in EN-1992 (2004), the bending moment values along the y and z axes are calculated as a function of a specified axial loading. The latter observation means that both bending moments are conditioned by the value of the acting axial loading and, therefore, the flexural capacity of RC cross-sections needs to be computed in the plane where P_x is constant, which is taken from the results of each Monte Carlo simulation.

5.2.2 FINITE ELEMENT MODEL FOR THE INTERACTION DOMAIN AND ITS VALIDATION

This section presents the numerical method to evaluate the response of RC cross-sections subjected to biaxial bending moments and axial loading. Such a procedure consists of implementing a zero-length nonlinear fibre section element in OpenSees with constitutive material models that can be more complex than those proposed by the technical standards (i.e., parabola-rectangle for the concrete and elastic-perfect plastic for the steel reinforcement). The following procedure determines the 3D-interaction domain (Figure 13):

- Definition of the nonlinear fibre RC section;
- Definition of the constitutive materials for the concrete and the steel reinforcement.
- Use of the MinMax material in OpenSees to constrain the values of the ultimate strains of concrete and steel rebars. (The MinMax material in OpenSees limits the values of the strain in compression and tension to obtain the endpoint of the moment-curvature);
- Definition of an angle (0-360 degrees) for the orientation of the loading axis. (the orientation of such loading axis is relevant for the definition of the incremental loading);
- Definition of a vector containing the axial loads (P);
- Calculation of the moment-curvature (M-χ) in the two local directions of the RC section for each axial load and its orientation;
- Definition of the maximum or the minimum bending moments (depending on the orientation of the loading axis) from the moment-curvature diagram in the two local directions;

- The maximum or the minimum moment in both directions are the pair of points defined on the interaction surface.

Figure 12 shows the 3D domain of a circular section of the Rio Torto bridge.

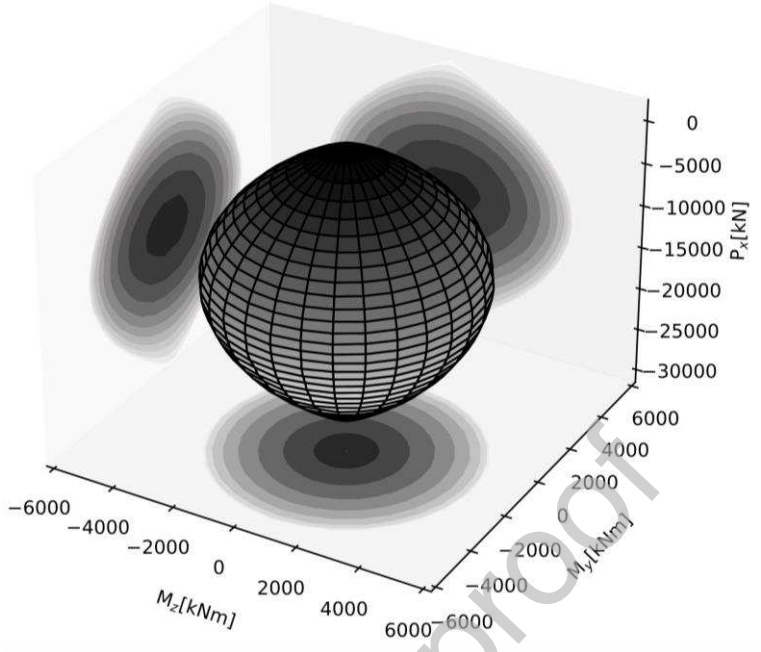

Figure 12. 3D Interaction domain of a circular column of the Rio Torto Bridge

The above-mentioned numerical procedure allows a proper definition of cross-section fibres, and there is no need for a simplification of the steel bar locations (due to computational issues, steel reinforcing bars often consist of only two layers, one in compression and one in tension). Furthermore, it considers the concrete cover and concrete core as independent materials, which produces more reliable and accurate results for the residual capacity of RC sections.

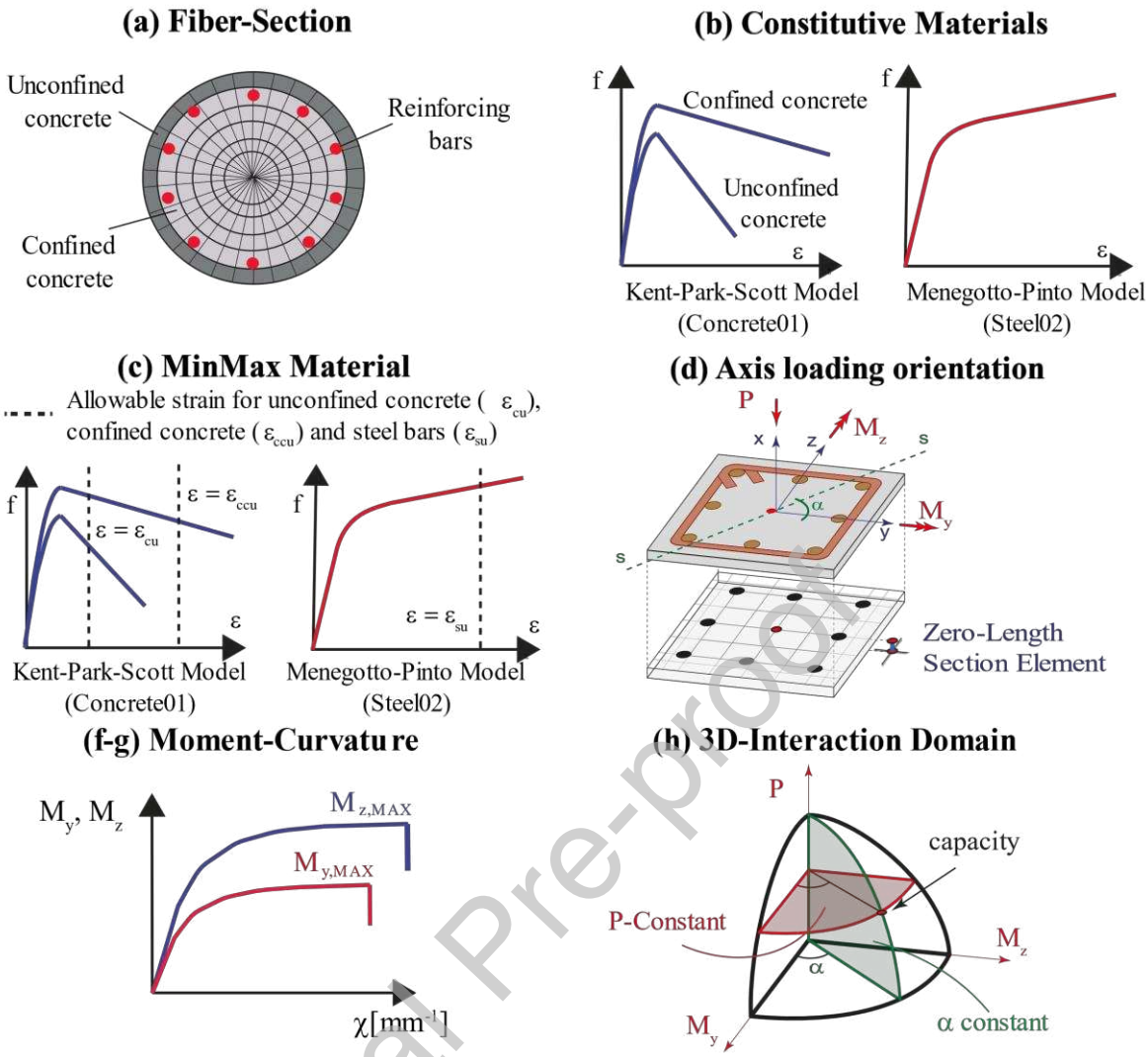

Figure 13. Layout of the numerical procedure for 3D interaction domains

It is imperative to accurately validate the proposed numerical method against experimental results available in the literature to prove its soundness and efficiency.

Several experimental studies were carried out on the behaviour of RC members under double or single eccentricity of the axial loading [e.g., Hsu (1986); Xia et al. (2016)], and are herein used to validate the proposed numerical method. Hsu (1988) conducted an experimental campaign on pristine RC elements with different shapes under biaxial bending moment, while Xia et al. (2016) used RC members under a uniaxial bending moment with different values of the corrosion rate. The deterioration modelling described previously in Section 4.1 is adopted for the mechanical and geometrical properties of the corroded RC members. The results of the numerical and experimental comparisons are illustrated in Figures 14 and 15.

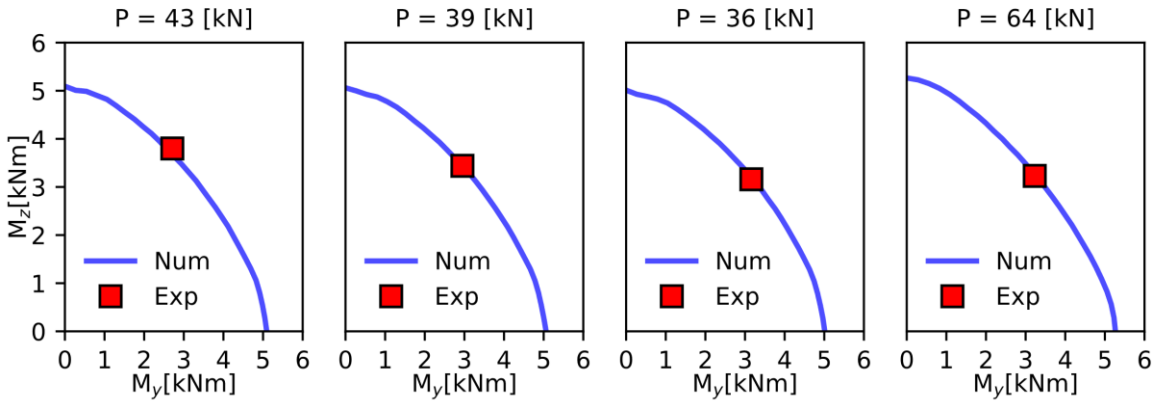

Figure 14. Experimental vs Numerical results (experimental results by [Hsu, (1988)], series U squared section 102x102 mm^2)

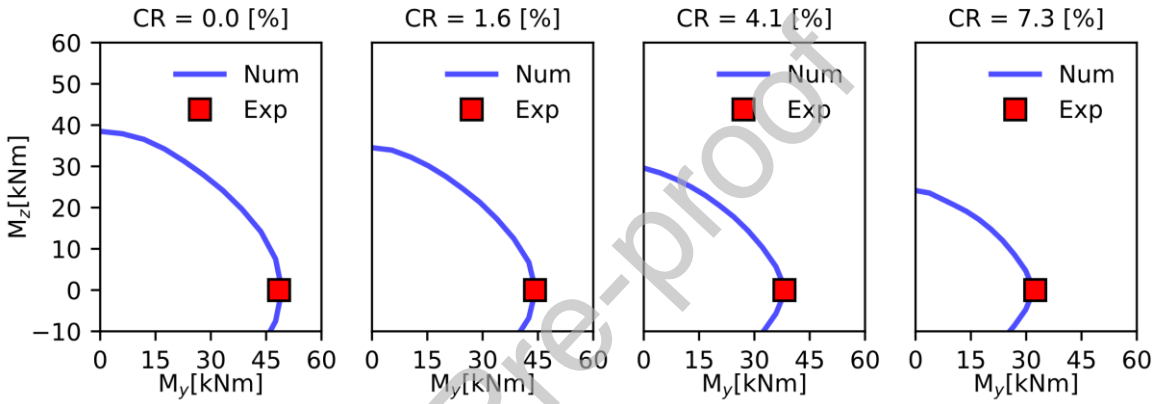

Figure 15. Experimental vs Numerical results (experimental results by [Xia et al., (2015)], series BS rectangular section 200x240 mm^2)

The numerical procedure can match the experimental tests with excellent accuracy, both for non-corroded and corroded RC members. Further details on the validation of such a procedure (in the 2D domain) can be found in Di Sarno and Pugliese (2020).

Finally, to investigate the effects of corrosion on the flexural strength and ductility of RC members, the moment-curvature diagrams of the experimental sample tests by Xia et al. (2016) are calculated. The ductility ($\mu = \chi_{ult}/\chi_{yield}$) is expressed by the ratio between the ultimate curvature (χ_{ult}) and the yielding (χ_{yield}) of an equivalent bilinear, while the strength by the maximum bending moments corresponding to the RC section.

The numerical results illustrated in Figures 16a and 16b show that corrosion significantly affects strength and ductility. Specifically, the strength shows a reduction from a maximum bending moment of 49.3 kNm to 44.3 kNm and from 49.3kNm to 32.0 kNm for the two examined case-studies (Figure 16a and 16b, respectively). Likewise, the ductility demonstrates a decay of 8.3% (Figure 16a) and 21.4% (Figure 16b) where the increase in the corrosion rate is 1.6% and 7.3%, respectively.

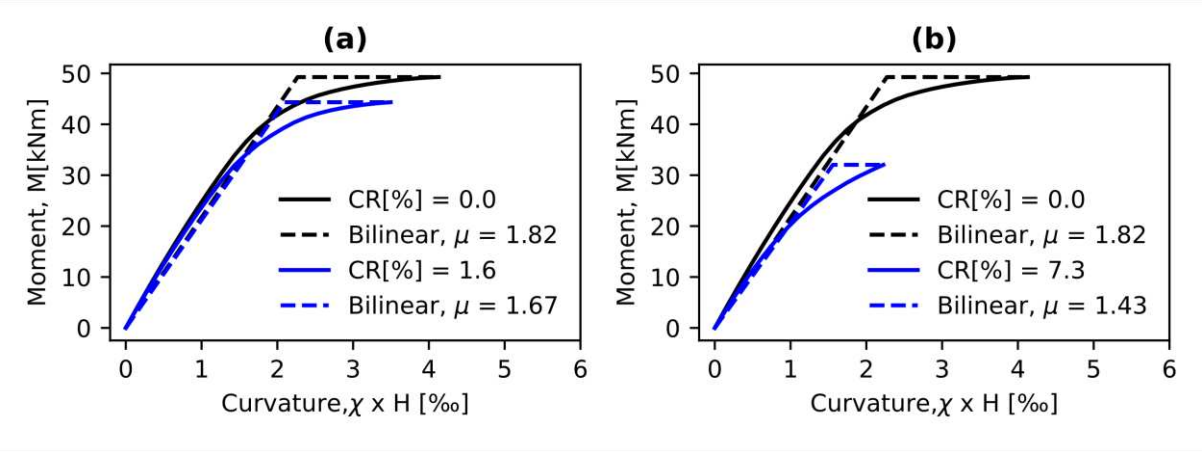

Figure 16. Moment Curvature. (a) RC member without and with corrosion: (a) CR [%] = 1.6 and (b) CR [%] = 7.3

5.3 RESPONSE SURFACE METHOD FOR SHEAR STRENGTH OF CORRODED RC COMPONENTS

Typically, corrosion reaches the transversal steel bar layers before the longitudinal ones. This latter reduces the confinement of an RC cross-section (and, thus, the concrete compressive strength) and lowers the global shear capacity of RC members [e.g., Xia et al. (2011); Zhu et al. (2013); Lachemi et al. (2014)].

The evaluation of the shear strength is not trivial for un-corroded RC components and becomes even more complex for corroded elements due to corrosion-related uncertainties. Performing regression analyses based on experimental tests available in the literature may entail various issues such as the digitalization of data and samples that do not comply with RC sections of existing bridges, among the others. Thus, a methodology capable of combining the accuracy between numerical and analytical approaches should be sought. Such a methodology is represented by the response surface of the model uncertainties.

The objective herein is to develop a surrogate model based on a well-established numerical approach that can efficiently define the shear capacity of corroded RC cross-sections. In this study, the numerical model named the modified compression field theory developed by Vecchio and Collin (1986) is used. This latter can predict the load-deformation relationships of RC members subjected to pure shear with excellent accuracy; hence, to obtain the shear prediction of each component, the software Response2000 [Bentz (2000)], based on the modified compression field theory and developed at the University of Toronto, is utilised. Such software allows users to analyse both beams and columns based on their geometrical and mechanical properties and subjected to axial, bending, and shear loadings.

Typically, the shear strength of RC components is defined as a function of three main contributions: (a) concrete, (b) transversal reinforcement, and (c) size aggregate. The contribution of size aggregate is yet here neglected and, therefore, the formulation holds as:

$$V_s = f\left(f_c\,, f_y\,, A_{st}\right) \tag{25}$$

where f_c , f_y , A_{st} (the area loss of the transversal reinforcement) are the input variables of the surrogate models. Monte Carlo simulations were performed to obtain as many combinations as possible for the input parameters and the shear strength. Once the combinations are acquired, the metamodel yields a function that simulates the numerical behaviour in the space

of random input variables. Such a numerical model (the modified compression field theory in this study) is then replaced by a first-order polynomial approximation (surrogate model), which describes the limit state function for the shear capacity of each examined RC section.

$$V_s = \alpha_0 + \sum_{i=1}^{n=2} \alpha_i x_i (f_c\,, f_y\, A_{st}) \tag{26}$$

The first-order polynomial formulation is fitted with standard regression analyses by adopting the function "regress" in Matlab (e.g., https://www.mathworks.com/help/stats/regress.html) [Liel et al. (2009)]. Such a function enables the representation of complex nonlinear combinations between input numerical model parameters and structural response of single components (shear capacity) in a simple linear relationship. For all RC sections, the linear response surface has the following form:

$$V_s = \alpha_0 + \alpha_1 f_c + \alpha_2 f_y A_{st} \tag{27}$$

The cross-validation method (k-fold) is adopted for estimating the expected error of the model. Such a method allows to split the data into k-folds (here assumed 5 and training-to-test ratio equal to 4) and fit and validate the model accordingly [Lallemant et al. (2015)]. The performance of the surrogate model for each RC cross-section is evaluated through the validation error defined as the normalised mean absolute error (NMAE) and shown in Figure 17.

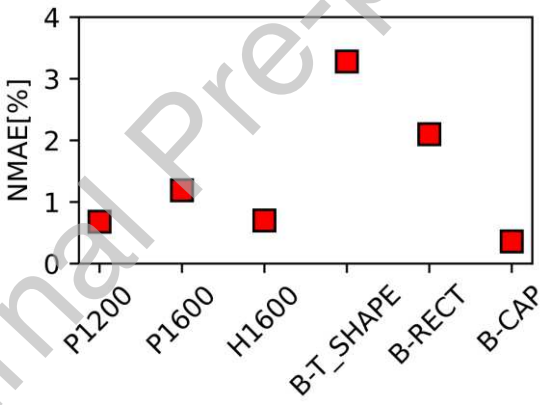

Figure 17. Cross-validation results. (Keynotes: P1200 and P1600- solid circular columns with 1200- and 1600-mm diameters, H1600 – hollow circular column with 1600mm diameter, B-T_SHAPE – beam with a t-shape section, B-RECT – beams with rectangular sections, B-CAP – cap beam).

The validation error shown in Figure 17 demonstrates the effectiveness of the surrogate model performance for each RC cross-section.

The interaction of the variables is graphically represented by the three-dimensional surfaces shown in Figure 18. Results illustrate that corrosion decreases the shear strength capacity of the RC section according to the reduction of the mechanical and geometrical properties of steel rebars and concrete. For instance, the cap-beam shear resistance is reduced by 20% compared to the pristine section, while such a reduction for circular columns is between 10-to-13%. The variation between beams and columns depends on the longitudinal reinforcement ratio, which is more significant for bridge piers.

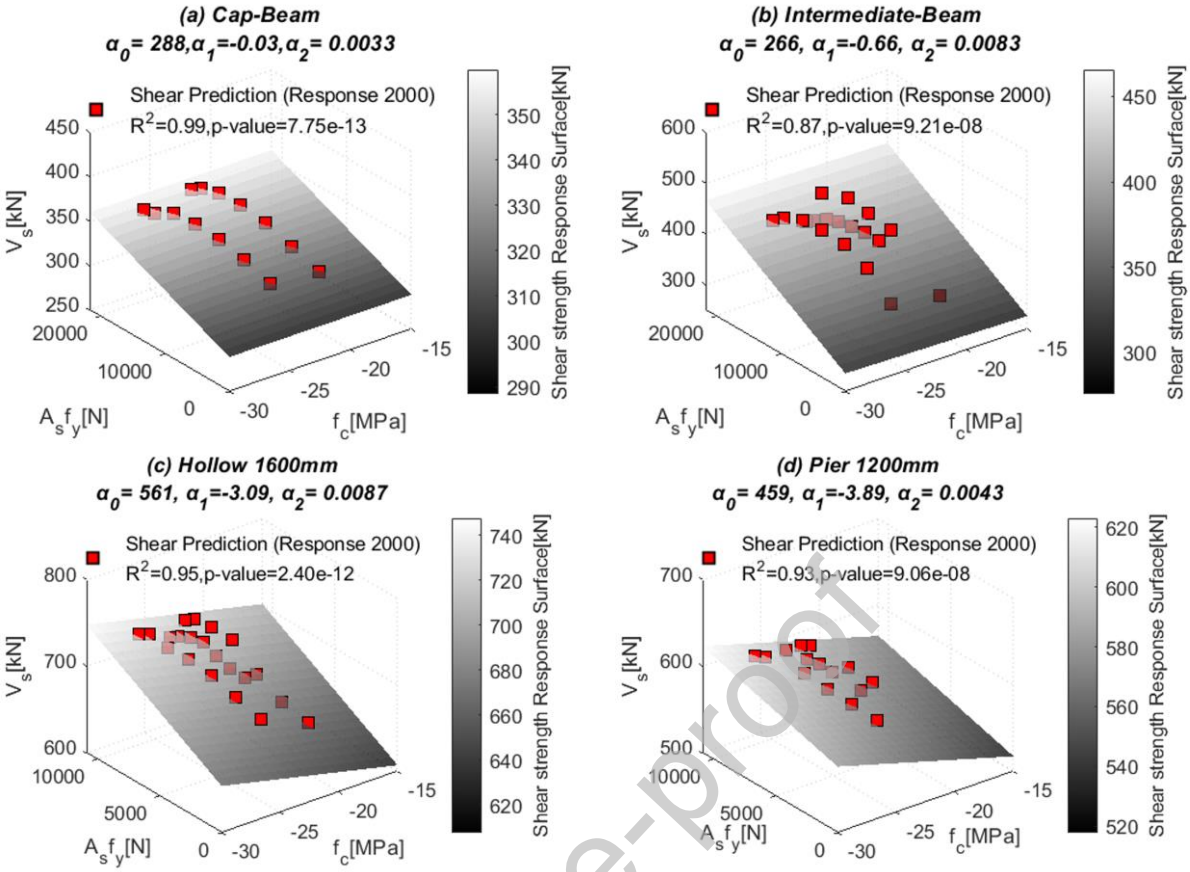

Figure 18. Response surface for the shear capacity of corroded RC sections

Furthermore, the effects of the axial loading are more relevant for RC columns than beams (it is negligible in this last case), as it can be seen in the relationship between the compressive strength (f_c) and the shear capacity (V_s) in Figures 18.

When the values of the shear capacity are obtained, the safety margin is calculated as:

$$G(t) = V_{SC} - V_{SD} \tag{28}$$

where V_{SD} is the shear demand and V_{SD} the shear capacity.

6. PROBABILISTIC TRAFFIC LOADING

The Rio Torto bridge was designed between 1960 and 1970 for a traffic loading of 20,000 vehicles per day. The growth of the economy, population, needs and the development of new vehicles have increased the traffic demand that the bridge is currently facing. As a result, both traffic flow prediction and traffic model are essential for its reliability assessment.

6.1 TRAFFIC DATA

The traffic demand analysis is extremely complex due to the significant variation of the unpredictable variables included in the data.

Hence, the traffic flow data are herein collected from a national database (www.autostrade.it) and are limited for the time span 1990-2020 (only this period is available from the database). Such data refer to the number of traffic attendants passing through the bridge per day and distinguish two vehicle categories (light with two axles and heavy with three axles). Figures 19 show that the light-over-heavy vehicle ratio (LHR) is roughly 2-to-1.

Two different regression methods are used to predict the vehicular traffic flow: (i) a power regression law ($veh = (year/a)^{1/b}$, $a = 1434.25$ *and* $b=0.031$) representing a continuous increase of the traffic demand and (ii) a logistic distribution ($veh = \frac{60000}{1+e^{-(a+bt)}}, a = -95.87$ *and* $b = 0.05$) representing a saturation condition (for the daily vehicular flow) that is three times the design value (Figure 19).

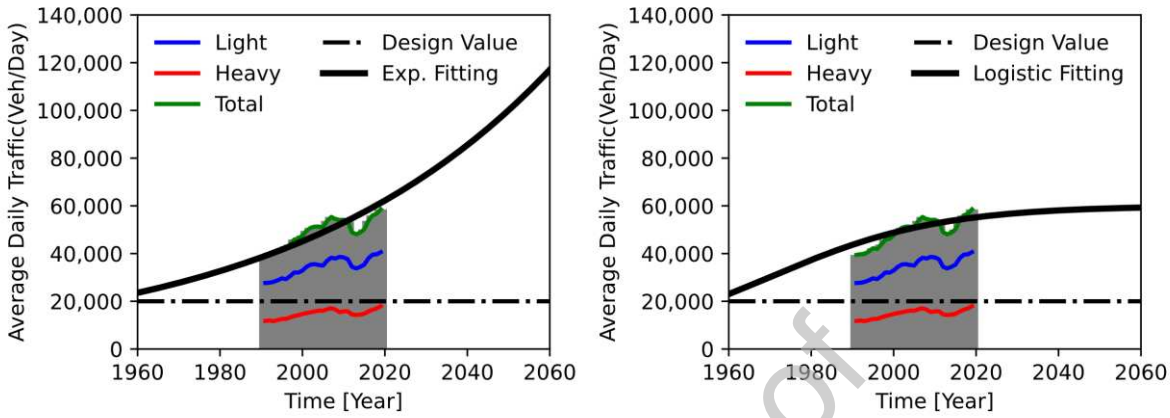

Figure 19. (a) Traffic data and (b) traffic flow prediction

6.2 STATIC TRAFFIC MODEL

The stochastic traffic loading (Figure 19) is generated such that each random traffic configuration is different from the previous one. The minimum velocity for the Italian motorways is commonly 50 km/h (i.e., 13.89 m/s); hence, dividing the length of the RC bridge (421.1 m) by the minimum velocity provides the maximum time taken from a vehicle to cross the bridge (i.e., 421.1m / 13.89ms^{-1} = 30.2 seconds). As a result, it is assumed that the traffic loading configuration changes every minute, which is a conservative assumption to account for any slower vehicles (less than 50km/h).

A uniform probabilistic distribution is then used to generate the random number of vehicles passing the bridge simultaneously. The lower bound (off-peak) of such a distribution is associated with the values predicted by either the power-law or logistic regression (Figure 19) for each examined year, while the upper bound is the maximum number of vehicles (on-peak) allowed by the bridge length. A minimum gap (headway) of 2 meters is imposed between cars, while the type of vehicles is generated assigning relative weights to light (70%) and heavy (30%) vehicles, according to the traffic data available in Figures 19.

Since the RC bridge model comprises one independent roadway, the traffic loading is simulated only in one direction and using two lanes. The probabilistic distributions of the headway, axle distance, and axle weight are derived from formulations available in the literature [e.g., Guo et al. (2012)]. The simply supported structural scheme assigns the vertical and the torsional load for each node that discretises the equivalent elastic beam deck (Figure 20). This latter is a simplification as it neglects the bending moments generated in each nodal mass of the bridge deck. However, such an assumption is compliant with the scope of the present study as the bending moment produced between no-supported nodal masses does not affect the deck behaviour (it is assumed an equivalent elastic beam element for the bridge deck) and becomes zero at the nodes supported by the bridge piers. As a result,

both configurations, with and without accounting for the bending moment, will lead to the same axial and torsional loads acting on the portal frames.

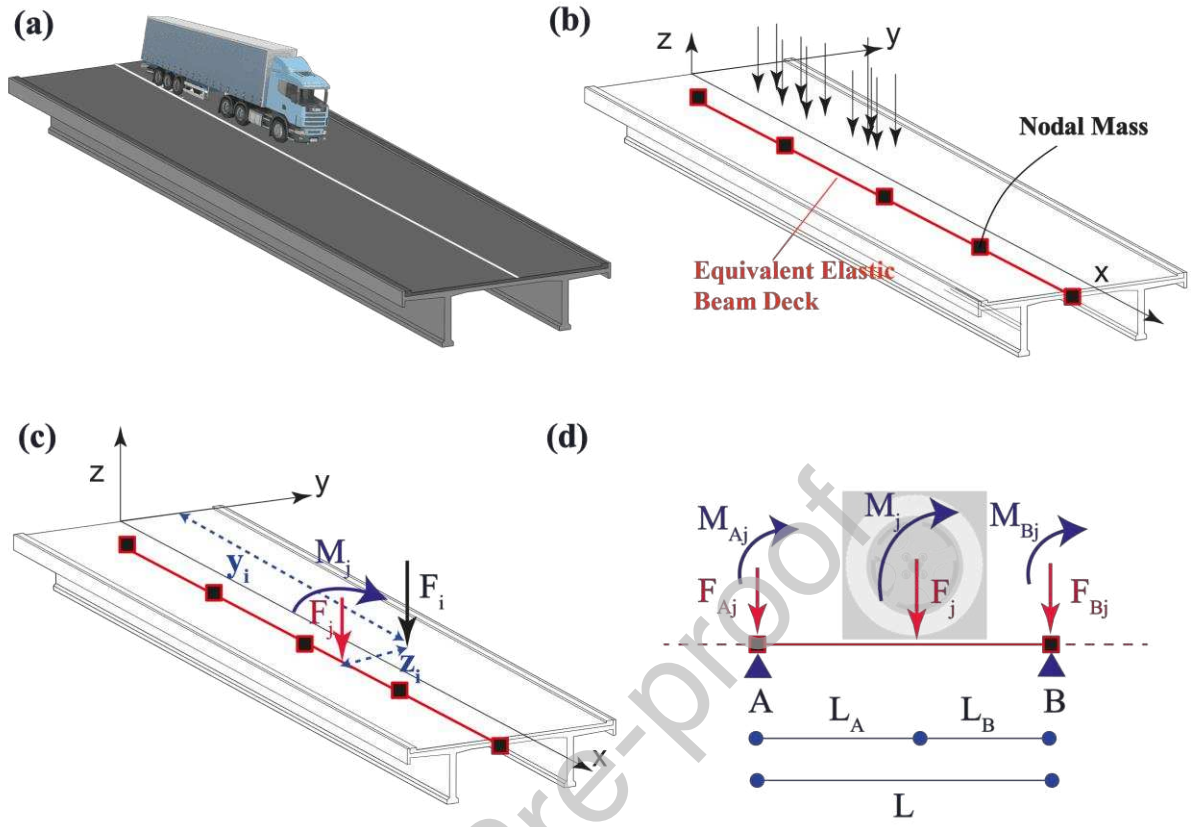

Figure 20. (a) Bridge deck, (b) Load model for each axle, (c) Loading on the equivalent elastic beam deck and (d) structural scheme for the traffic loading

Once the traffic loading configuration is applied to the bridge model, the static analysis is performed to calculate the internal forces of each element composing the portal frame.
The approach presented above is a simplification with respect to more sophisticated dynamic modelling [e.g., De Risi (2021)]; however, it is deemed suitable for the case study at hand.

7. RESULTS

The reliability assessment is carried out by performing static analyses of the RC bridge at intervals of 10 years with 100,000 Monte Carlo simulations. Such analyses allow to estimate the reliability index of each RC component and, ultimately, of each portal frame pier. Such reliability indices are then compared to the corresponding values provided by EN-1990 (2002).
The basic principles stated in the EN-1990 (2002) and other international codes [e.g., AASHTO (2014)], consider target reliability indices corresponding to specific reference times (T_s); typically, one and fifty years. In this study, the RC bridge falls in the category "RC3" [EN-1990 (2002)], which accounts for either high consequences of human life or high social and economic impact; thus, the target indices are 5.2 and 4.3 for one and fifty years, respectively. Therefore, the target reliability index is time-variant; thus, assuming that the failure probability is independent year-by-year, the following approximation can be used:

$$p_f(t) = 1-\left[1 - p_{f1}\right]^{T_S/T_1} \quad (33)$$

where p_{f1} is the failure probability calculated at t = 1 year. The failure probability calculated in Eq. (33) can be converted into the corresponding reliability index using Eq. (21).

Figures 21 and 22 show the reliability analysis results for all four case scenarios (exponential and logistic traffic demand with complete and zero correlation). Only the minimum envelope of the reliability indices is reported for the sake of clarity.

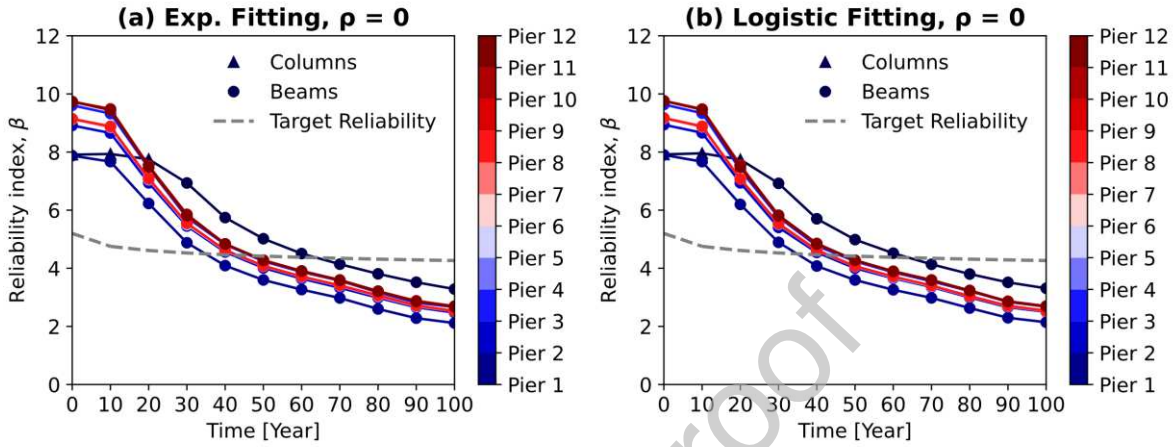

Figure 21. Reliability index for ρ=0: (a) Exponential and (b) Logistic traffic growth

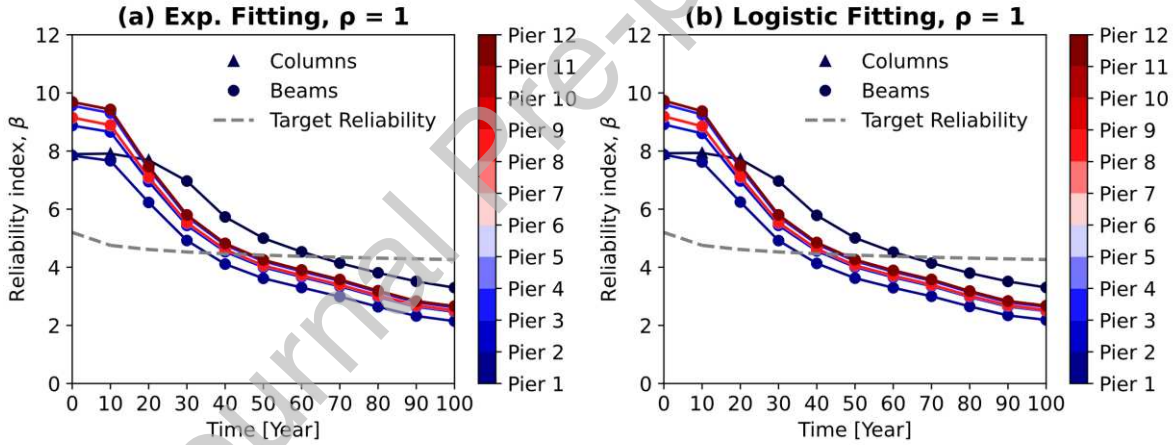

Figure 22. Reliability index for ρ=1: (a) Exponential and (b) Logistic traffic growth

Results show a significant reduction of the reliability index over time. Corrosion has the primary effect and is predominant over the traffic flow conditions for this specific bridge. The flexural failure mode governs the reliability, while the shear never reaches the target reliability.

Figure 23 shows the variation of the shear-over-flexure reliability index ratios ($\beta_{shear}/\beta_{flexure}$) with time. The results demonstrate that the shear reliability index is always higher than the flexural one.

RC beams are mainly subjected to simple bending, and the effects of corrosion on the structural capacity of RC beams are significantly larger than the ones on RC columns. This is because RC columns are subjected to higher axial loadings due to the self-weight and the increased traffic demand, which leads to smaller failure probabilities.

Pier 2 shows the smallest reliability index over time, which is initially between 7.87 and 7.84 (ρ=0 and ρ=1, respectively) for the exponential traffic loading and 7.90 and 7.88 (ρ=0 and ρ=1, respectively) for the logistic traffic loading, respectively. Such values decrease at 2.14 and 2.11 (ρ=0 and ρ=1, respectively) and 2.18 and 2.14 (ρ=0 and ρ=1, respectively) at the time of 100 years for the exponential and logistic traffic demand, respectively. Such a decrease yields a reduction of the structural capacity of about 72%. Furthermore, the reliability indices are slightly different between the two correlation scenarios and depend upon the traffic flow condition. The complete correlation is more conservative as the geometrical/mechanical properties, and the corrosion characteristics are assigned once for all bridge piers; for instance, if CR =100%, this will be applied to all portal frames. About the traffic flow, the exponential fitting produces heavier traffic demands and higher internal forces, increasing the failure probability.

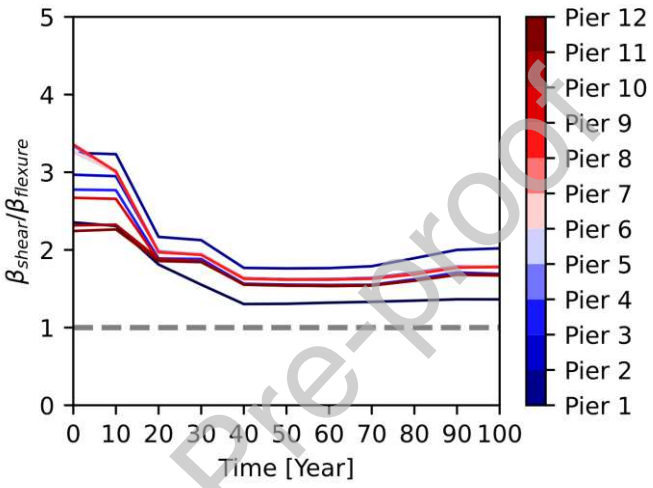

Figure 23 Brittle-over-ductile reliability index

Pier 1 shows a slight decrease in the reliability index up to 20 years (from 7.92 to 7.72 on average) with columns governing the flexural failure mode and a progressive decay up to 3.28 at a time of 100 years with beams governing the failure mode.

Piers 3 and 4 have distinct behaviour as they are made of different RC cross-sections. The reliability index values for Pier 3 are 8.91 and 8.87 (ρ=0 and ρ=1, respectively) at the construction time and 2.48 and 2.46 at a time of 100 years for the increasing traffic scenario. Similarly, the logistic traffic case-study produces a reliability index from 8.94 and 8.91 (ρ=0 and ρ=1, respectively) to 2.51 and 2.49 (ρ=0 and ρ=1, respectively). Conversely, Pier 4 yields values from 9.61 and 9.56 (ρ=0 and ρ=1, respectively) to 2.66 and 2.61 (ρ=0 and ρ=1, respectively) for the exponential traffic demand and, from 9.63 and 9.61 to 2.68 to 2.63 for the logistic traffic loading. Such a difference between Pier 4 and Pier 3 depends on the fact that Pier 3 has larger beams.

Piers 5, 6, 7, 8 and 9 exhibit similar results in the failure probability as the failure mode is governed by the rectangular cross-section beams. The total reliability index ranges on average from 9.18 for the pristine bridge to 2.52 at the end of the bridge lifetime. This latter indicates a total decrease of 75% compared to the non-corroded sample bridge.

Likewise, the failure probability for Piers 10, 11 and 12 is determined by the flexural failure of the intermediate beams; however, Pier 10-to-12 have lower failure probabilities. Specifically, β ranges averagely from 9.69 at the beginning of the bridge construction to 2.66

at the end of the bridge life. Complete correlation across piers provides a further reduction of the reliability index equal to 3% compared to zero correlation, while a 6% is determined between exponential and logistic traffic demands (2.66 and 2.70, respectively).
The numerical results of each portal frame and traffic flow demonstrate that corrosion reduces the reliability index by 93% for such a type of RC bridge, while the relative decrease due to the various traffic conditions over time is not higher than 7%.
Therefore, to investigate the effects of the correlation factors used to simulate the spatial variability of corrosion, the variation between the two case studies is shown in Figure 24 and computed for the worst scenario (t = 100 years) as follows:

$$Variation(\%) = \frac{\beta(t = 100\ yrs)_{\rho=0} - \beta(t = 100yrs)_{\rho=1}}{\beta(t = 100yrs)_{\rho=0}} \quad (34)$$

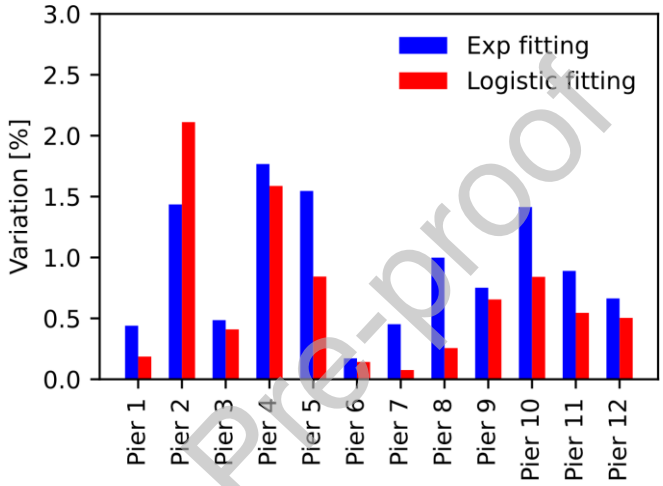

Figure 24. Variation in the structural correlation of corrosion

The variation in Figure 24 demonstrates that the correlation factors do not contribute significantly to the reliability index of the bridge studied herein. Future studies should investigate the reliability index over time, assuming correlation factors between pier components rather than among piers, if those are portal frames.
Finally, the maintenance interventions (in years) given by the intersections between the target reliability index over time (dashed lines in Figures 21 and 22) and the reliability index from the numerical simulations of each portal frame are plotted in Figure 25.
Piers 1 and 2 show the highest and lowest time for maintenance interventions, 64 and 35 (on average) years, respectively. Conversely, Piers 3 and 4 require maintenance at 42 and 46 years, and Piers 5-to-9 at 43 years. Finally, Piers 10, 11 and 12 reach the target reliability at around 47 years.
It is worth noticing that once the failure probability over time has been quantified, it can be multiplied by a proper cost-utility metric to assess the risk associated with a specific failure event. Such a risk assessment can then be used to obtain a decision variable for decision-making strategies and optimal maintenance schemes.

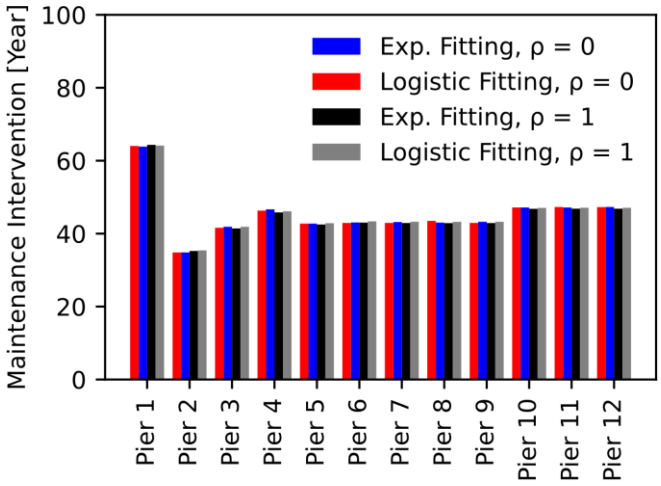

Figure 25. Maintenance interventions

8. CONCLUSIONS AND FUTURE WORKS

The reliability analysis of an existing thirteen-bay RC bridge was conducted to investigate the effects of the increasing traffic loading demand and spatially variable corrosion over time. A probabilistic approach was developed to estimate the time initiation, propagation, and deterioration. The temperature data from a local database for a specific time interval were used to identify the minimum and maximum temperature cycle effects on the environmental factor and, thus, on the corrosion stages. The three-dimensional interaction domain and the shear capacity surface response were obtained to calculate the capacity of each RC component. Finally, the reliability indices from the numerical analyses were compared against the values provided by EN-1990 (2002). From the comprehensive parametric study, the following conclusions can be drawn:

- The lognormal distribution having mean variable with cover-to-diameter ratio and a constant standard deviation is appropriate to describe the critical pit depth along the steel reinforcement bars;
- The generalised extreme value distribution can accurately describe the pitting factor;
- The minimum and maximum average temperatures for a specific time interval can be described via a generalised extreme value distribution and adopted to calculate the environmental factor;
- The environmental factor can be modelled with a gamma distribution. The results indicated that climatic-related phenomena could reduce the corrosion occurrence time, i.e., from 28 years to 26 years;
- A uniform distribution for evaluating the severe cracking width seems to be a good trade-off between available experimental results and formulations available from technical standards;
- The lognormal distribution could adequately describe the critical crack width that leads to the concrete cover spalling. This distribution showed that the basic assumption of 1 mm for the crack inducing the spalling is quite conservative;
- The comparison of available experimental flexural failures and the failure model proposed herein proves the reliability and the efficiency of the developed tool to predict the flexural capacity of corroded and non-corroded RC components;

- The surrogate model for the shear strength of corroded RC components, based on the modified compressive field theory and the statistical significance parameters presented in Figure 18, showed that such a methodology a practical analytical tool;
- The traffic flow data could be adequately modelled by a power-law regression and a logistic law regression based on monitored data from a national database;
- The results from the reliability analysis showed that the numerical reliability index decreased over time. Pier 2 illustrated the lowest reliability, with a total decrease of 72% at the end of the bridge lifetime compared to the pristine bridge. On the other hand, Pier 1 showed the highest reliability index from 7.28 to 3.30. The predominant failure mode for Pier 1 was the flexure of the RC columns up to 20 years; afterwards, RC beams governed the structural failure. Piers 3 and 4 produced different reliability indices, mainly due to stronger beams included in Pier 3. Piers 5-to-9 showed similar behaviour with β from 9.2 for the pristine bridge to 2.52 at 100 years with a total decrease of 75% for the structural capacity of the portal frames. Likewise, Piers 10-to-12 had a dominant flexural failure of the rectangular beams. Unlike Piers 5-to-9, the reliability index was slightly higher over time;
- Flexure was the predominant failure of each portal frame composing the sample bridge. In particular, the normalised reliability index in Figure 23 shows that the shear safety margin is always higher than the flexural one for gravity analyses;
- The comparison of the reliability index values for the complete and zero correlation illustrated that the effects of corrosion are so severe as to reduce the effects of the correlation. Further studies should focus on numerical analyses where the random field is applied to single components of each pier rather than studying correlation among piers;
- The bridge piers reached the target reliability at different times, ranging between 65 years (Pier 1) and 34 years (Pier 2). The remaining Piers (3-to-12) illustrated a maintenance intervention between 42 years and 47 years. Such results are relevant for decision-making strategies and optimal maintenance schemes;
- Further studies should investigate the reliability index profile obtained using more sophisticated statistical distributions than the uniform distribution to simulate the on-peak and off-peak traffic flow;
- Such a holistic approach, based on a comprehensive reliability framework, represents a step forward for a proper evaluation of the post-earthquake response and viability of existing RC bridges [Ghasemi and Lee (2021)] due to its flexibility to be integrated with other natural hazard analyses (i.e., earthquakes, winds, and floods).

This study suggests that future experimental and numerical studies should focus on the crack width leading to cover spalling. The probabilistic distribution provided in this manuscript appears to be quite an improvement compared to the basic assumption in the literature.

Appendix A

Table A1. Statistical distribution of the model parameters in Eq. (2).
(*keynotes*: μ and σ for the lognormal distribution are the mean and the standard deviation of the associated normal distribution , *w/b* – It is assumed 0.5 in this study; *Beta (a, b, lw, up)* is a beta distribution with *a* and *b* shape parameters, and *lw* and *up* lower and upper bounds, respectively; *Gamma (μ, σ)* is a gamma distribution with shape parameter $\alpha = \left(\frac{\mu}{\sigma}\right)^2$ and scale parameter $\beta = \frac{\sigma^2}{\mu}$)

Parameter	Description	Distribution Name				
			μ	σ		
X_1	***Model Uncertainty***	Lognormal (μ, σ)	1	0.05		
			μ	σ		
D_{Cl}	***Chloride Diffusion Coefficient***	Normal (μ, σ)	$15.8 \cdot 10^{-12}$ (m^2/s)	0.2μ		
			μ	σ		
k_e	***Environmental Factor***	Gamma (μ, σ)	0.676	0.114		
			μ	σ		
kt	***test method factor***	Normal (μ, σ)	0.832	0.024		
			a	b	l_w	u_p
kc	***Execution Factor***	Beta (a, b, lw, up)	4.445	2.333	0.400	1.000
t_0	***Reference time***	Deterministic	0.0767 yr			
			μ	σ		
C_{crit}	***Critical Chloride Content***	Normal (μ, σ)	0.5	0.1		
C_{S0}	***Surface Chloride Concentration***					
It is calculated as a function of the water-to-binder ratio (w/b=0.5): $C_{S0} = A_{S0}$ (w/b) + ε_{S0}.						
			μ	σ		
A_{S0}	***Chloride content regression parameter***	Normal (μ, σ)	2.565	0.356		
			μ	σ		
ε_{S0}	***Error term for the chloride concentration***	Normal (μ, σ)	0	0.405		
			a	b	lw	up
n_{cl}	***Age Factor***	Beta (a, b, l_w, u_p)	4.075	9.508	0.000	1.000

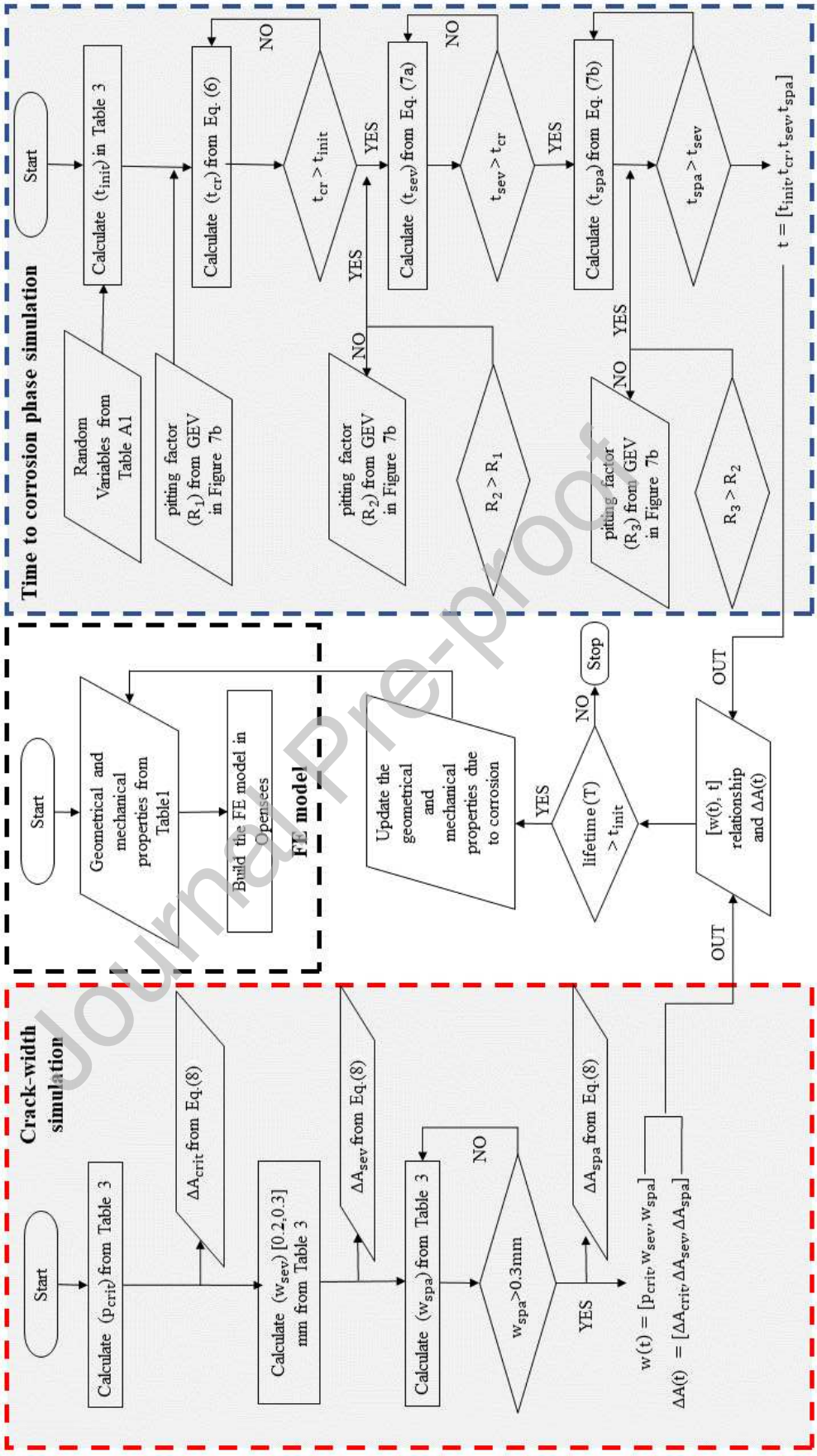

Figure A1. Layout of the Corrosion Numerical Procedure

Declaration of interest

The authors declare that they have no known competing financial interests or personal relationships that could have appeared to influence the work reported in this paper.

ACKNOWLEDGEMENTS

The authors would like to acknowledge the gracious support of this work through the EPSRC and ESRC Centre for Doctoral Training on Quantification and Management of Risk and Uncertainty in Complex Systems Environments Grant No. (EP/L015927/1). The second author is supported by the Engineering and Physical Sciences Research Council (EPSRC) project UKCRIC (EP/R012806/1). This work was undertaken on Barkla, part of the High-Performance Computing facilities at the University of Liverpool, UK, and using the computational facilities of the Advanced Computing Research Center, University of Bristol (http://www.bris.ac.uk/acrc/).

AUTHORS' CONTRIBUTION

First Author: Conceptualization; Methodology; Software programming; Analysis; Post-processing; Data collection; Resources, Writing the original draft; **Second Author**: Conceptualization; Methodology; Software programming; Resources; Review and editing. **Third Author**: Conceptualization; Supervision; Research Team leader; Review and editing.

References

1. AASHTO (American Association of State Highway and Transportation Officials). (2014). AASHTO LRFD Bridge Design Specifications. *Washington, DC*.
2. Abbiati, G., Bursi, O. S., Caperan, P., Di Sarno, L., Molina, F. J., Paolacci, F., & Pegon, P. (2015). Hybrid simulation of a multi-span RC viaduct with plain bars and sliding bearings. *Earthquake Engineering & Structural Dynamics, 44*, 2221–2240.
3. Akiyama, M., & Frangopol, D. M. (2014). Long-term seismic performance of RC structures in an aggressive environment: Emphasis on bridge piers. *Structure and Infrastructure Engineering, 10*, 865–879.
4. Akiyama, M., Frangopol, D. M., & Matsuzaki, H. (2011). Life-cycle reliability of RC bridge piers under seismic and airborne chloride hazards. *Earthquake Engineering & Structural Dynamics, 40*, 1671–1687.
5. Alonso, C., Andrade, C., Rodriguez, J., & Diez, J. M. (1998). Factors controlling cracking of concrete affected by reinforcement corrosion. *Materials and structures, 31*, 435–441.
6. Andisheh, K., Scott, A., & Palermo, A. (2019). Experimental evaluation of the residual compression strength and ultimate strain of chloride corrosion-induced damaged concrete. *Structural Concrete, 20*, 296–306.
7. Ang, A. H., & Tang, W. H. (2007). Probability concepts in engineering: emphasis on applications to civil and environmental engineering. *John Wiley & Sons Incorporated*.
8. Arismendi, R., Barros, A., & Grall, A. (2021). Piecewise deterministic Markov process for condition-based maintenance models—Application to critical infrastructures with discrete-state deterioration. *Reliability Engineering & System Safety, 212*, 107540.

9. Bentz, E. C. (2000). *Sectional analysis of reinforced concrete members.* University of Toronto Toronto.

10. Calvert, G., Neves, L., Andrews, J., & Hamer, M. (2020). Multi-defect modelling of bridge deterioration using truncated inspection records. *Reliability Engineering & System Safety, 200*, 106962.

11. Caprani, C. C., & O'Brien, E. J. (2006). Finding the distribution of bridge lifetime load effect by Predictive Likelihood. *3rd International ASRANet Colloquium, held at the University of Glasgow, 10-12 July 2006.*

12. Celik, O. C., & Ellingwood, B. R. (2010). Seismic fragilities for non-ductile reinforced concrete frames–Role of aleatoric and epistemic uncertainties. *Structural Safety, 32*, 1–12.

13. Chan, T. H., Miao, T. J., & Ashebo, D. B. (2005). Statistical models from weigh-in-motion data. *Structural Engineering and Mechanics, 20*, 85–110.

14. Chen, S., Lu, L., Xiang, Y., Lu, Q., & Li, M. (2018). A data heterogeneity modeling and quantification approach for field pre-assessment of chloride-induced corrosion in aging infrastructures. *Reliability Engineering & System Safety, 171*, 123–135.

15. Choe, D.-E., Gardoni, P., Rosowsky, D., & Haukaas, T. (2009). Seismic fragility estimates for reinforced concrete bridges subject to corrosion. *Structural Safety, 31*, 275–283.

16. Coronelli, D., & Gambarova, P. (2004). Structural assessment of corroded reinforced concrete beams: modeling guidelines. *Journal of structural engineering, 130*, 1214–1224.

17. Cui, F., Zhang, H., Ghosn, M., & Xu, Y. (2018). Seismic fragility analysis of deteriorating RC bridge substructures subject to marine chloride-induced corrosion. *Engineering Structures, 155*, 61–72.

18. De Larrard, T., Bastidas-Arteaga, E., Duprat, F., & Schoefs, F. (2014). Effects of climate variations and global warming on the durability of RC structures subjected to carbonation. *Civil Engineering and Environmental Systems, 31*, 153–164.

19. De Risi, R. (2021). A computational framework for finite element modeling of traveling loads on bridges in dynamic regime. *Computer-Aided Civil and Infrastructure Engineering.*, 1-15. doi:10.1111/mice.12745

20. De Risi, R., Di Sarno, L., & Paolacci, F. (2017). Probabilistic seismic performance assessment of an existing RC bridge with portal-frame piers designed for gravity loads only. *Engineering Structures, 145*, 348–367.

21. Di Sarno, L., & Pugliese, F. (2020). Numerical evaluation of the seismic performance of existing reinforced concrete buildings with corroded smooth rebars. *Bulletin of Earthquake Engineering, 18*, 4227–4273.

22. Di Sarno, L., Pugliese, F., & De Risi, R. (2021). Non-linear finite element optimization for inelastic buckling modelling of smooth rebars. *Engineering Structures*, 240, 112378.

23. Ditlevsen, O., & Madsen, H. O. (1996). *Structural reliability methods* (Vol. 178). Wiley New York.

24. DuraCrete. (2000). Statistical quantification of the variables in the limit state functions. *The European Union-Brite EuRam III-Contract BRPR-CT95-0132-Project BE95-1347/R9*.

25. Ellingwood, B. R. (2005). Risk-informed condition assessment of civil infrastructure: state of practice and research issues. *Structure and infrastructure engineering, 1*, 7–18.

26. EN, B. S. (1992). 1-1: 2004 Eurocode 2: Design of concrete structures. *General rules and rules for buildings, 3*.

27. EN, C. E. (1990). Eurocode–Basis of Structural Design, 2002. *Eurocode–Basis of Structural Design, 2002*. IBN-BIN.

28. Enright, B., & O'Brien, E. J. (2013). Monte Carlo simulation of extreme traffic loading on short and medium span bridges. *Structure and Infrastructure Engineering, 9*, 1267–1282.

29. Enright, M. P., & Frangopol, D. M. (1998). Service-life prediction of deteriorating concrete bridges. *Journal of Structural engineering, 124*, 309–317.

30. Fabbrocino, G., Verderame, G. M., & Manfredi, G. (2005). Experimental behaviour of anchored smooth rebars in old type reinforced concrete buildings. *Engineering Structures, 27*, 1575–1585.

31. Frangopol, D. M., Strauss, A., & Kim, S. (2008). Bridge reliability assessment based on monitoring. *Journal of Bridge Engineering, 13*, 258–270.

32. Ghasemi, S. H., & Lee, J. Y. (2021). Reliability-based indcator for post-earthquake traffic flow capacity of a highway bridge. *Structural Safety, 89*, 102039.

33. Ghosh, J., & Padgett, J. E. (2010). Aging considerations in the development of time-dependent seismic fragility curves. *Journal of Structural Engineering, 136*, 1497–1511.

34. Ghosh, J., & Sood, P. (2016). Consideration of time-evolving capacity distributions and improved degradation models for seismic fragility assessment of aging highway bridges. *Reliability Engineering & System Safety, 154*, 197–218.

35. Gong, C., & Frangopol, D. M. (2019). An efficient time-dependent reliability method. *Structural Safety, 81*, 101864.

36. Guo, T., Frangopol, D. M., & Chen, Y. (2012). Fatigue reliability assessment of steel bridge details integrating weigh-in-motion data and probabilistic finite element analysis. *Computers & Structures, 112*, 245–257.

37. Hsu, C.-T. T. (1988). Analysis and design of square and rectangular columns by equation of failure surface. *Structural Journal, 85*, 167–179.

38. Imperatore, S., Rinaldi, Z., & Drago, C. (2017). Degradation relationships for the mechanical properties of corroded steel rebars. *Construction and Building Materials, 148*, 219–230.

39. Jalayer, F. (2003). *Direct probabilistic seismic anaysis: implementing non-linear dynamic assessments.* Ph.D. dissertation, Stanford University Stanford, CA.

40. Jalayer, F., De Risi, R., & Manfredi, G. (2015). Bayesian Cloud Analysis: efficient structural fragility assessment using linear regression. *Bulletin of Earthquake Engineering, 13*, 1183–1203.

41. Kumar, R., Gardoni, P., & Sanchez-Silva, M. (2009). Effect of cumulative seismic damage and corrosion on the life-cycle cost of reinforced concrete bridges. *Earthquake Engineering & Structural Dynamics, 38*, 887–905.

42. Lachemi, M., Al-Bayati, N., Sahmaran, M., & Anil, O. (2014). The effect of corrosion on shear behavior of reinforced self-consolidating concrete beams. *Engineering structures, 79*, 1–12.

43. Lallemant, D., Kiremidjian, A., & Burton, H. (2015). Statistical procedures for developing earthquake damage fragility curves. *Earthquake Engineering & Structural Dynamics, 44*, 1373–1389.

44. Liel, A. B., Haselton, C. B., Deierlein, G. G., & Baker, J. W. (2009). Incorporating modeling uncertainties in the assessment of seismic collapse risk of buildings. *Structural Safety, 31*, 197–211.

45. McKenna, F., Fenves, G. L., Scott, M. H., & others. (2000). Open system for earthquake engineering simulation. *University of California, Berkeley, CA*.

46. Monteiro, R., Delgado, R., & Pinho, R. (2016). Probabilistic seismic assessment of RC bridges: part I—uncertainty models. *Structures*, *5*, pp. 258–273.

47. Nesterova, M., Schmidt, F., & Soize, C. (2020). Fatigue analysis of a bridge deck using the peaks-over-threshold approach with application to the Millau viaduct. *SN Applied Sciences, 2*, 1–12.

48. O'connor, A., & O'Brien, E. J. (2005). Traffic load modelling and factors influencing the accuracy of predicted extremes. *Canadian Journal of Civil Engineering, 32*, 270–278.

49. Pan, Q., Grimmelsman, K., Moon, F., & Aktan, E. (2011). Mitigating epistemic uncertainty in structural identification: Case study for a long-span steel arch bridge. *Journal of Structural Engineering, 137*, 1–13.

50. Paolacci, F., Pegon, P., Molina Ruiz, F., Poljansek, M., Giannini, R., Di Sarno, L., . . . Yenidogan, C. (2014). Assessment of the seismic vulnerability of an old RC viaduct with frame piers and study of the effectiveness of base isolation through PsD testing (RETRO). *SERIES Transnational Access report. EUR 26471. Luxembourg (Luxembourg): Publications Office of the European Union*.

51. Razvi, S., & Saatcioglu, M. (1999). Confinement model for high-strength concrete. *Journal of Structural Engineering, 125*, 281–289.

52. Rodriguez, J., Ortega, L. M., & Casal, J. (1996). Load bearing capacity of concrete columns with corroded reinforcement. *CORROSION OF REINFORCEMENT IN CONCRETE CONSTRUCTION. PROCEEDINGS OF FOURTH INTERNATIONAL SYMPOSIUM, CAMBRIDGE, 1-4 JULY 1996. SPECIAL PUBLICATION NO 183.*

53. Rodriguez, J., Ortega, L. M., & Casal, J. (1997). Load carrying capacity of concrete structures with corroded reinforcement. *Construction and building materials, 11*, 239–248.

54. Shekhar, S., & Ghosh, J. (2020). A metamodeling based seismic life-cycle cost assessment framework for highway bridge structures. *Reliability Engineering & System Safety, 195*, 106724.

55. Shome, N. (1999). *Probabilistic seismic demand analysis of nonlinear structures.* Stanford University.

56. Simon, J., Bracci, J. M., & Gardoni, P. (2010). Seismic response and fragility of deteriorated reinforced concrete bridges. *Journal of Structural Engineering, 136*, 1273–1281.

57. Spacone, E., Filippou, F. C., & Taucer, F. F. (1996). Fibre beam–column model for non-linear analysis of R/C frames: Part I. Formulation. *Earthquake Engineering & Structural Dynamics, 25*, 711-725. doi:https://doi.org/10.1002/(SICI)1096-9845(199607)25:7<711::AID-EQE576>3.0.CO;2-9

58. Spacone, E., Filippou, F. C., & Taucer, F. F. (1996b). Fibre beam–column model for non-linear analysis of R/C frames: part II. Applications. *Earthquake Engineering & Structural Dynamics, 25*, 727–742.

59. Stewart, M. G., & Al-Harthy, A. (2008). Pitting corrosion and structural reliability of corroding RC structures: Experimental data and probabilistic analysis. *Reliability engineering & system safety, 93*, 373–382.

60. Stewart, M. G., Wang, X., & Nguyen, M. N. (2011). Climate change impact and risks of concrete infrastructure deterioration. *Engineering Structures, 33*, 1326–1337.

61. Strauss, A., Wendner, R., Bergmeister, K., & Costa, C. (2013). Numerically and experimentally based reliability assessment of a concrete bridge subjected to chloride-induced deterioration. *Journal of Infrastructure Systems, 19*, 166–175.

62. Thanapol, Y., Akiyama, M., & Frangopol, D. M. (2016). Updating the seismic reliability of existing RC structures in a marine environment by incorporating the spatial steel corrosion distribution: Application to bridge piers. *Journal of Bridge Engineering, 21*, 04016031.

63. Thoft-Christensen, P. (2000). Stochastic modeling of the crack initiation time for reinforced concrete structures. In *Advanced technology in structural engineering* (pp. 1–8).

64. Torres-Acosta, A. A., & Mart ı´ nez-Madrid, M. (2003). Residual life of corroding reinforced concrete structures in marine environment. *Journal of Materials in Civil Engineering, 15*, 344–353.

65. Val, D. V., & Melchers, R. E. (1997). Reliability of deteriorating RC slab bridges. *Journal of structural engineering, 123*, 1638–1644.

66. Vecchio, F. J., & Collins, M. P. (1986). The modified compression-field theory for reinforced concrete elements subjected to shear. *ACI J., 83*, 219–231.

67. Verderame, G. M., Ricci, P., De Carlo, G., & Manfredi, G. (2009). Cyclic bond behaviour of plain bars. Part I: Experimental investigation. *Construction and Building Materials, 23*, 3499–3511.

68. Verderame, G. M., Stella, A., & Cosenza, E. (2001). Le proprietà meccaniche degli acciai impiegati nelle strutture in ca realizzate negli anni'60. *X Congresso Nazionale L'ingegneria Sismica in Italia, Potenza-Matera*, (pp. 9–13).

69. Vidal, T., Castel, A., & François, R. (2004). Analyzing crack width to predict corrosion in reinforced concrete. *Cement and concrete research, 34*, 165–174.

70. Xia, J., Jin, W.-l., & Li, L.-y. (2011). Shear performance of reinforced concrete beams with corroded stirrups in chloride environment. *Corrosion Science, 53*, 1794–1805.

71. Xia, J., Jin, W.-L., & Li, L.-Y. (2016). Performance of corroded reinforced concrete columns under the action of eccentric loads. *Journal of materials in civil Engineering, 28*, 04015087.

72. Yang, D. Y., & Frangopol, D. M. (2020). Life-cycle management of deteriorating bridge networks with network-level risk bounds and system reliability analysis. *Structural Safety, 83*, 101911.

73. Yanweerasak, T., Pansuk, W., Akiyama, M., & Frangopol, D. M. (2018). Life-cycle reliability assessment of reinforced concrete bridges under multiple hazards. *Structure and Infrastructure Engineering, 14*, 1011–1024.

74. Yu, L., Francois, R., Dang, V. H., L'Hostis, V., & Gagne, R. (2015). Distribution of corrosion and pitting factor of steel in corroded RC beams. *Construction and Building Materials, 95*, 384–392.

75. Zhang, P. S., Lu, M., & Li, X. Y. (1995). The mechanical behaviour of corroded bar. *Journal of Industrial Buildings, 25*, 41–44.

76. Zhong, J., Gardoni, P., & Rosowsky, D. (2010). Stiffness degradation and time to cracking of cover concrete in reinforced concrete structures subject to corrosion. *Journal of engineering mechanics, 136*, 209–219.

77. Zhou, X.-Y., Schmidt, F., Toutlemonde, F., & Jacob, B. (2016). A mixture peaks over threshold approach for predicting extreme bridge traffic load effects. *Probabilistic Engineering Mechanics, 43*, 121–131.

78. Zhu, W., François, R., Coronelli, D., & Cleland, D. (2013). Effect of corrosion of reinforcement on the mechanical behaviour of highly corroded RC beams. *Engineering Structures, 56*, 544–554.